Atmosphere Modeling I: Intro & Dynamics

-the CAM (Community Atmosphere Model) dynamical cores

Peter Hjort Lauritzen

Atmospheric Modeling & Predictability Section (AMP)
Climate and Global Dynamics Laboratory (CGD)
National Center for Atmospheric Research (NCAR)

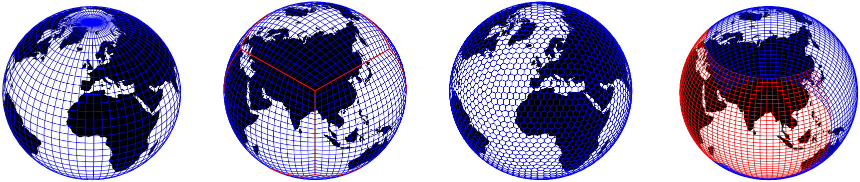

This material is based upon work supported by the National Center for Atmospheric Research, which is a major facility sponsored by the National Science Foundation under Cooperative Agreement No. 1852977.

1. Atmosphere intro
   - Discretization grid: Resolved and un-resolved scales
   - Multi-scale nature of atmosphere dynamics
   - 'Define' dynamical core and parameterizations

2. CAM-FV dynamical core (CESM2 'work horse' dynamical core for $\approx 1^\circ$ applications)
   - Horizontal and vertical grid
   - Continuous Equations of motion
   - Finite-volume discretization of the equations of motion
     - The Lin & Rood (1996) advection scheme

3. Next generation dynamical core options in CAM
   - CAM-SE(Spectral-Elements)-CSLAM(Conservative Semi-LAgrangian Multi-tracer scheme): Planned as next default dynamical core for 1° climate applications
   - CAM-MPAS(Model for Prediction Across Scales) and CAM-FV3(cubed-sphere FV)

Domain

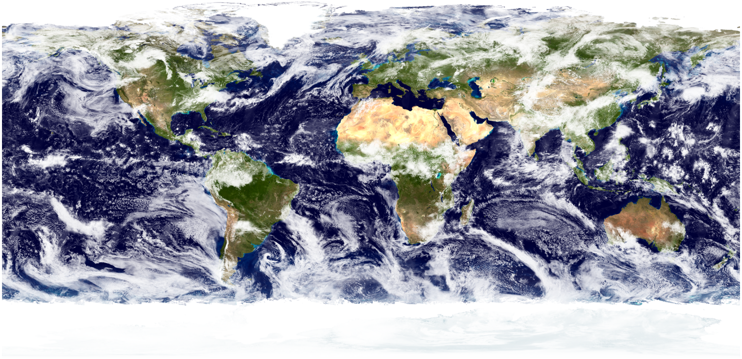

Source: NASA Earth Observatory

Horizontal computational space

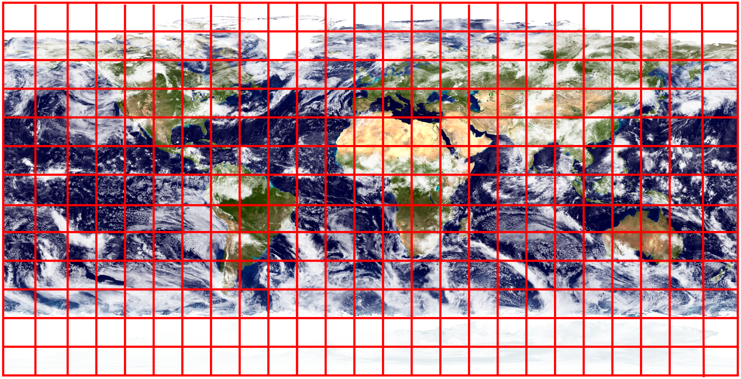

- Red lines: regular latitude-longitude grid
- Grid-cell size defines the smallest scale that can be resolved ($\neq$ **effective resolution!**)
- Many important processes taking place sub-grid-scale that must be parameterized
- Loosely speaking, the parameterizations compute grid-cell average tendencies due to sub-grid-scale processes in terms of the (resolved scale) atmospheric state
- In modeling jargon parameterizations are also referred to as *physics* (what is unphysical about resolved scale dynamics?)

Effective resolution: smallest scale (highest wave-number $k = k_{eff}$) that a model can accurately represent

- k_{eff} can be assessed analytically for linearized equations (Von Neumann analysis)
- In a full model one can assess k_{eff} using total kinetic energy spectra (TKE) of, e.g., horizontal wind $\vec{v}$ (see Figure below)

Effective resolution is typically 4-10 grid-lengths depending on numerical method!
$\Rightarrow$ be careful analyzing phenomena at the grid scale (e.g., extremes)

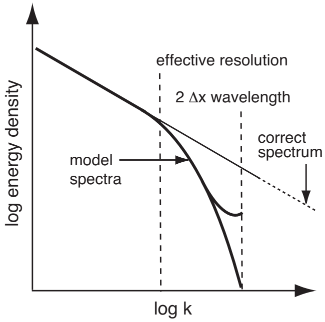

Figure from Skamarock (2011): Schematic depicting the possible behavior of spectral tails derived from model forecasts.

Horizontal computational space

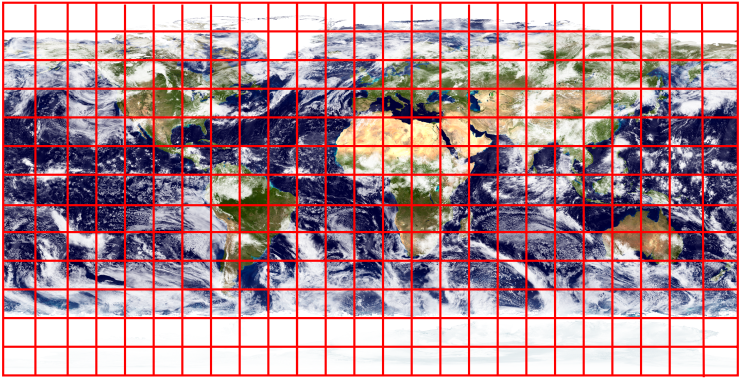

- Red lines: regular latitude-longitude grid
- Grid-cell size defines the smallest scale that can be resolved ($\neq$ **effective resolution!**)
- Many important processes taking place sub-grid-scale that must be parameterized
- Loosely speaking, the parameterizations compute grid-cell average tendencies due to sub-grid-scale processes in terms of the (resolved scale) atmospheric state
- In modeling jargon parameterizations are also referred to as *physics* (what is unphysical about resolved scale dynamics?)

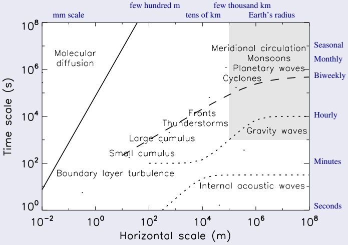

Figure indicates schematically the time scales and horizontal spatial scales of a range of atmospheric phenomena (Figure from Thuburn 2011).

Multi-scale nature of atmosphere dynamics (from Thuburn 2011)

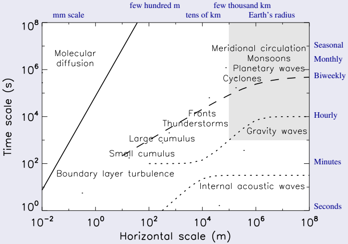

Figure indicates schematically the time scales and horizontal spatial scales of a range of atmospheric phenomena (Figure from Thuburn 2011).

- $\mathcal{O}(10^4\,km)$: large scale circulations (Asian summer monsoon).

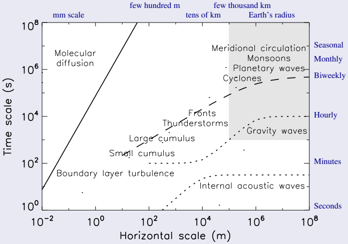

Figure indicates schematically the time scales and horizontal spatial scales of a range of atmospheric phenomena (Figure from Thuburn 2011).

- $\mathcal{O}(10^4 km)$: large scale circulations (Asian summer monsoon).
- $\mathcal{O}(10^4 km)$: undulations in the jet stream and pressure patterns associated with the largest scale Rossby waves (called *planetary waves*)

Multi-scale nature of atmosphere dynamics (from Thuburn 2011)

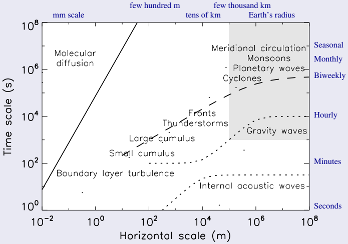

Figure indicates schematically the time scales and horizontal spatial scales of a range of atmospheric phenomena (Figure from Thuburn 2011).

- $\mathcal{O}(10^4 km)$: large scale circulations (Asian summer monsoon).
- $\mathcal{O}(10^4 km)$: undulations in the jet stream and pressure patterns associated with the largest scale Rossby waves (called *planetary waves*)
- $\mathcal{O}(10^3 km)$: cyclones and anticyclones

Multi-scale nature of atmosphere dynamics (from Thuburn 2011)

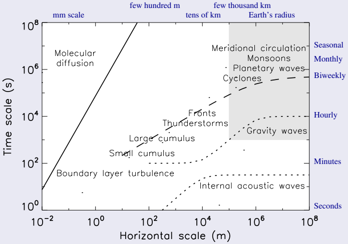

Figure indicates schematically the time scales and horizontal spatial scales of a range of atmospheric phenomena (Figure from Thuburn 2011).

- $\mathcal{O}(10^4 km)$: large scale circulations (Asian summer monsoon).
- $\mathcal{O}(10^4 km)$: undulations in the jet stream and pressure patterns associated with the largest scale Rossby waves (called *planetary waves*)
- $\mathcal{O}(10^3 km)$: cyclones and anticyclones
- $\mathcal{O}(10 km)$: the transition zones between relatively warm and cool air masses can collapse in scale to form fronts with widths of a few tens of km

Multi-scale nature of atmosphere dynamics (from Thuburn 2011)

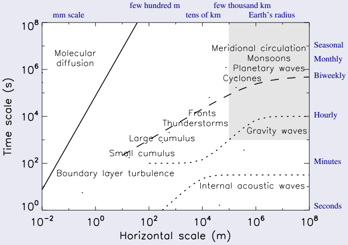

Figure indicates schematically the time scales and horizontal spatial scales of a range of atmospheric phenomena (Figure from Thuburn 2011).

- $\mathcal{O}(10^4 km)$: large scale circulations (Asian summer monsoon).
- $\mathcal{O}(10^4 km)$: undulations in the jet stream and pressure patterns associated with the largest scale Rossby waves (called *planetary waves*)
- $\mathcal{O}(10^3 km)$: cyclones and anticyclones
- $\mathcal{O}(10 km)$: the transition zones between relatively warm and cool air masses can collapse in scale to form fronts with widths of a few tens of km
- $\mathcal{O}(10^3 km - 100 m)$: convection can be organized on a huge range of different scales (tropical intraseasonal oscillations; supercell complexes and squall lines; individual small cumulus clouds formed from turbulent boundary layer eddies)

Multi-scale nature of atmosphere dynamics (from Thuburn 2011)

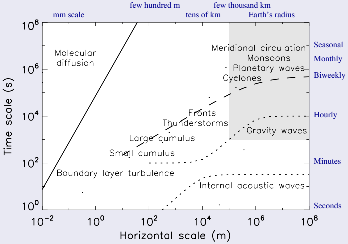

Figure indicates schematically the time scales and horizontal spatial scales of a range of atmospheric phenomena (Figure from Thuburn 2011).

- $\mathcal{O}(10^4 km)$: large scale circulations (Asian summer monsoon).
- $\mathcal{O}(10^4 km)$: undulations in the jet stream and pressure patterns associated with the largest scale Rossby waves (called *planetary waves*)
- $\mathcal{O}(10^3 km)$: cyclones and anticyclones
- $\mathcal{O}(10 km)$: the transition zones between relatively warm and cool air masses can collapse in scale to form fronts with widths of a few tens of km
- $\mathcal{O}(10^3 km - 100m)$: convection can be organized on a huge range of different scales (tropical intraseasonal oscillations; supercell complexes and squall lines; individual small cumulus clouds formed from turbulent boundary layer eddies)
- $\mathcal{O}(10m - 1mm)$: turbulent eddies in boundary layer (lowest few hundred m's of the atmosphere, where the dynamics is dominated by turbulent transports); range in scale from few hundred m's (the boundary layer depth) down to *mm* scale at which molecular diffusion becomes significant.

Multi-scale nature of atmosphere dynamics (from Thuburn 2011)

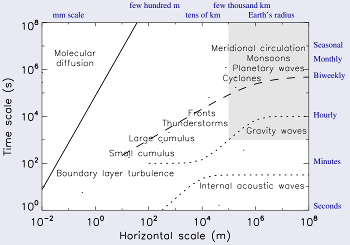

- All of the phenomena along the dashed line are important for weather and climate, and so need to be represented in numerical models.
- Important phenomena occur at all scales - there is no significant *spectral gap*! Moreover, there are strong interactions between the phenomena at different scales, and these interactions need to be represented.
- The lack of any spectral gap makes the modeling of weather/climate very challenging

- $\mathcal{O}(10^4 km)$: large scale circulations (Asian summer monsoon).
- $\mathcal{O}(10^4 km)$: undulations in the jet stream and pressure patterns associated with the largest scale Rossby waves (called *planetary waves*)
- $\mathcal{O}(10^3 km)$: cyclones and anticyclones
- $\mathcal{O}(10 km)$: the transition zones between relatively warm and cool air masses can collapse in scale to form fronts with widths of a few tens of km
- $\mathcal{O}(10^3 km - 100 m)$: convection can be organized on a huge range of different scales (tropical intraseasonal oscillations; supercell complexes and squall lines; individual small cumulus clouds formed from turbulent boundary layer eddies)
- $\mathcal{O}(10 m - 1 mm)$: turbulent eddies in boundary layer (lowest few hundred m's of the atmosphere, where the dynamics is dominated by turbulent transports); range in scale from few hundred m's (the boundary layer depth) down to mm scale at which molecular diffusion becomes significant.

Multi-scale nature of atmosphere dynamics (from Thuburn 2011)

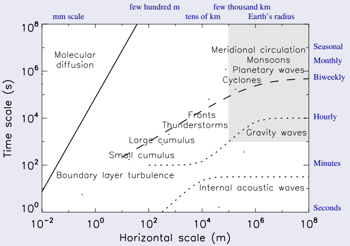

- Two dotted curves correspond to dispersion relations for gravity waves and internal acoustic waves (relatively fast processes)
- these lines lie significantly below the energetically dominant processes on the dashed line
  - $\Rightarrow$ they are energetically weak compared to the dominant processes along the dashed curve
  - $\Rightarrow$ we do relatively little damage if we distort their propagation
  - the fact that these waves are fast puts constraints on the size of Δt (at least for explicit and semi-implicit time-stepping schemes)!

- $\mathcal{O}(10^4 km)$: large scale circulations (Asian summer monsoon).
- $\mathcal{O}(10^4 km)$: undulations in the jet stream and pressure patterns associated with the largest scale Rossby waves (called *planetary waves*)
- $\mathcal{O}(10^3 km)$: cyclones and anticyclones
- $\mathcal{O}(10 km)$: the transition zones between relatively warm and cool air masses can collapse in scale to form fronts with widths of a few tens of km
- $\mathcal{O}(10^3 km - 100 m)$: convection can be organized on a huge range of different scales (tropical intraseasonal oscillations; supercell complexes and squall lines; individual small cumulus clouds formed from turbulent boundary layer eddies)
- $\mathcal{O}(10 m - 1 mm)$: turbulent eddies in boundary layer (lowest few hundred m's of the atmosphere, where the dynamics is dominated by turbulent transports); range in scale from few hundred m's (the boundary layer depth) down to mm scale at which molecular diffusion becomes significant.

Multi-scale nature of atmosphere dynamics (from Thuburn 2011)

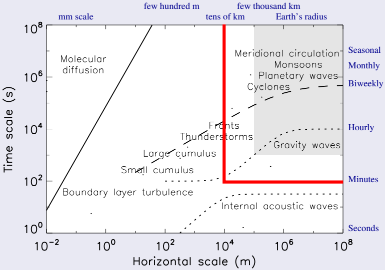

Horizontal resolution:

- the shaded region shows the resolved space/time scales in typical current day climate models (approximately $1^{O} - 2^{O}$ resolution)
- highest resolution at which uniform resolution CAM is run/developed is on the order of $10 - 25km$
- as the resolution is increased some 'large-scale' parameterizations may no longer be necessary (e.g., large scale convection) and we might need to redesign some parameterizations that were developed for horizontal resolutions of hundreds of km's (**grey zone!**)
- DYAMOND simulations: $\sim 5km$ or higher resolution (Stevens et al., 2019)

- $\mathcal{O}(10^4 km)$: large scale circulations (Asian summer monsoon).
- $\mathcal{O}(10^4 km)$: undulations in the jet stream and pressure patterns associated with the largest scale Rossby waves (called *planetary waves*)
- $\mathcal{O}(10^3 km)$: cyclones and anticyclones
- $\mathcal{O}(10 km)$: the transition zones between relatively warm and cool air masses can collapse in scale to form fronts with widths of a few tens of km
- $\mathcal{O}(10^3 km - 100m)$: convection can be organized on a huge range of different scales (tropical intraseasonal oscillations; supercell complexes and squall lines; individual small cumulus clouds formed from turbulent boundary layer eddies)
- $\mathcal{O}(10m - 1mm)$: turbulent eddies in boundary layer (lowest few hundred m's of the atmosphere, where the dynamics is dominated by turbulent transports); range in scale from few hundred m's (the boundary layer depth) down to mm scale at which molecular diffusion becomes significant.

Model code

Parameterization suite

- Moist processes: deep convection, shallow convection, large-scale condensation
- Radiation and Clouds: cloud microphysics, precipitation processes, radiation
- Turbulent mixing: planetary boundary layer parameterization, vertical diffusion, gravity wave drag

'Resolved' dynamics

'Roughly speaking, the **dynamical core** solves the governing fluid and thermodynamic equations on resolved scales, while the parameterizations represent sub-grid-scale processes and other processes not included in the dynamical core such as radiative transfer.' - Thuburn (2008)

Model code

Parameterization suite

- Moist processes: deep convection, shallow convection, large-scale condensation
- Radiation and Clouds: cloud microphysics, precipitation processes, radiation
- Turbulent mixing: planetary boundary layer parameterization, vertical diffusion, gravity wave drag

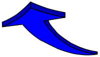

Strategies for coupling:

- process-split: dynamical core & parameterization suite are based on the same state and their tendencies are added to produce the updated state (used in CAM-EUL)
- time-split: dynamic core & parameterization suite are calculated sequentially, each based on the state produced by the other (used in CAM-FV; the order matters!).
- different coupling approaches discussed in the context of CCM3 in Williamson (2002)
- simulations are very dependent on coupling time-step (e.g. Williamson and Olson, 2003)
- (re-)emerging research topic: physics-dynamics coupling (PDC) conference series (Gross et al., 2018)

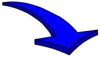

'Resolved' dynamics

'Roughly speaking, the **dynamical core** solves the governing fluid and thermodynamic equations on resolved scales, while the parameterizations represent sub-grid-scale processes and other processes not included in the dynamical core such as radiative transfer.' - Thuburn (2008)

Spherical (horizontal) discretization grid ($\sim 1^\circ$)

CAM-FV uses regular latitude-longitude grid:

- horizontal resolution specified when creating a new case:

```
./create_newcase -res res ...
```

  where, e.g., res=f09_f09_mg17 which is the $\Delta\lambda \times \Delta\theta = 0.9^\circ \times 1.25^\circ$ horizontal resolution configuration of the FV dynamical core corresponding to nlon=288, nlat=192.

  Changing resolution requires rebuilding (not a namelist variable).

- Note: Convergence of the meridians near the poles.

Spherical (horizontal) discretization grid ($\sim 1^\circ$)

CAM-SE (Spectral-Elements) and CAM-SE-CSLAM (Conservative Semi-LAgrangian Multi-tracer scheme) use (gnomonic) cubed-sphere grid:

```
./create_newcase -res ne30_ne30_mg17 or ne30pg3_ne30pg3_mg17
```

where `neXX` refers to number of elements along a cubed-sphere side and `pgX` refers to separate physics/tracer grid (next slide).

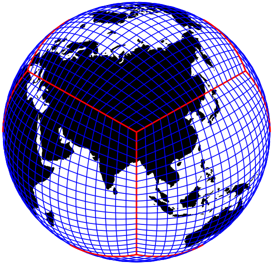

CAM-SE-CSLAM (Herrington et al., 2018, 2019) - ne30pg3_ne30pg3_mg17

CAM-SE has the option to run physics on a finite-volume grid that is coarser, same or finer resolution compared to the dynamics grid. This configuration uses inherently conservative CSLAM (Conservative Semi-LAgrangan Multi-tracer) transport scheme (Lauritzen et al., 2017).

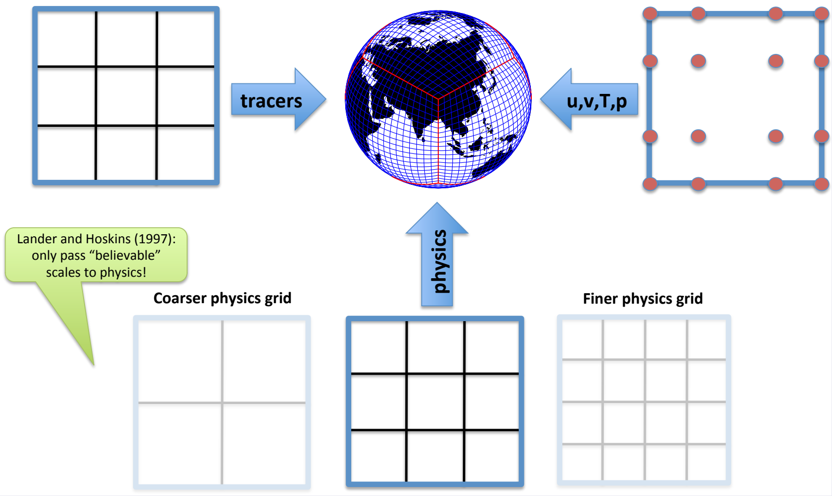

Spherical (horizontal) discretization grid ($\sim 1^\circ$)

CAM-MPAS (Model for Prediction Across Scales) uses a Voronoi grid:

```
./create_newcase -res mpasa120_mpasa120
```

where 120 refers to ~120km resolution.

Spherical (horizontal) discretization grid ($\sim 1^\circ$)

CAM-FV3, loosely speaking, a cubed-sphere version of CAM-FV:

```
./create_newcase -res C96_C96_mg17
```

where CXX refers to number of control volumes along a cubed-sphere side.

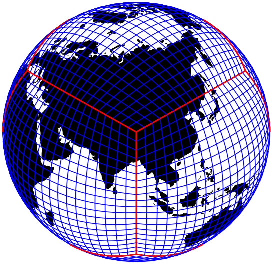

Spherical (horizontal) discretization grid ($\sim 1^\circ$)

PLEASE NOTE

Having several dynamical cores in the same framework makes CAM/CESM very unique!

You can seamlessly switch between dynamical cores which enables lots of interesting science, e.g.,

- study sensitiviy to dynamical core (using the exact same physics package and setup)
- CESM simpler models research (easily run baroclinic waves and other idealized configurations with all the dynamical cores)
  You don't have to spend months hacking the code to do your research in idealized modeling!
- make "apples to apples" performance comparisons
- facilitates/enables numerical methods research

Example of baroclinic waves with different dynamical cores:

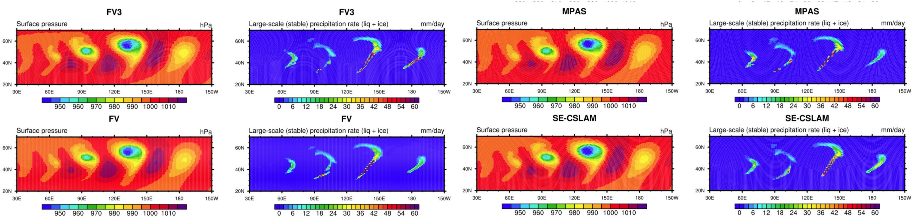

Vertical coordinate: hybrid sigma ($\sigma = p/p_s$)-pressure (p) coordinate

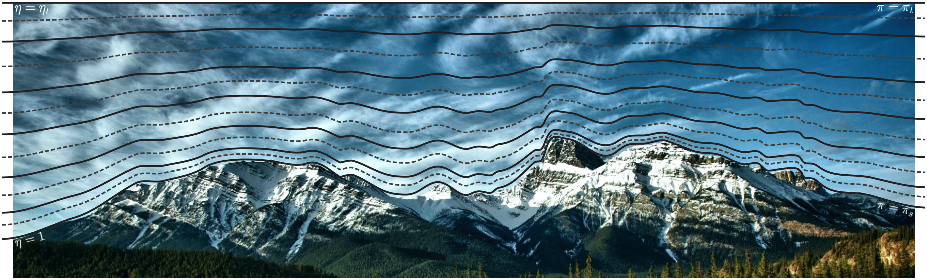

Figure courtesy of David Hall (CU Boulder).

Sigma layers at the bottom (following terrain) with isobaric (pressure) layers aloft.

Pressure at model level interfaces

$$p_{k+1/2} = A_{k+1/2}\, p_0 + B_{k+1/2}\, p_s,$$

where p_s is surface pressure, p_0 is the model top pressure, and $A_{k+1/2}(\in [0:1])$ and $B_{k+1/2}(\in [1:0])$ hybrid coefficients (in model code: *hyai* and *hybi*). Similarly for model level mid-points.

Note: vertical index is 1 at model top and *klev* at surface.

- CAM-FV,SE and FV3 use a Lagrangian ('floating') vertical coordinate ξ so that

$$\frac{d\xi}{dt} = 0,$$

i.e. vertical surfaces are material surfaces (no flow across them).

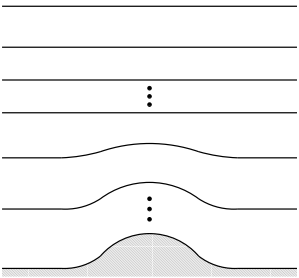

Figure shows 'usual' hybrid $\sigma - p$ vertical coordinate $\eta(p_s, p)$ (where p_s is surface pressure):

- $\eta(p_s, p)$ is a monotonic function of p.
- $\eta(p_s, p_s) = 1$
- $\eta(p_s, 0) = 0$
- $\eta(p_s, p_{top}) = \eta_{top}$.

Boundary conditions are:

- $\frac{d\eta(p_s,p_s)}{dt} = 0$
- $\frac{d\eta(p_s,p_{top})}{dt} = \omega(p_{top}) = 0$

(ω is vertical velocity in pressure coordinates)

Vertical coordinate

- CAM-FV,SE and FV3 use a Lagrangian ('floating') vertical coordinate ξ so that

$$\frac{d\xi}{dt} = 0,$$

i.e. vertical surfaces are material surfaces (no flow across them).

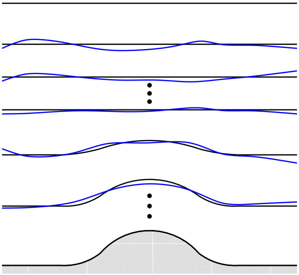

Figure:

- set $\xi = \eta$ at time t_{start} (black lines).
- for $t > t_{start}$ the vertical levels deform as they move with the flow (blue lines).
- to avoid excessive deformation of the vertical levels (non-uniform vertical resolution) the prognostic variables defined in the Lagrangian layers ξ are periodically remapped (= conservative interpolation) back to the Eulerian reference coordinates η.

Why use floating Lagrangian vertical coordinates?
Vertical advection terms disappear (3D model becomes 'stacked shallow-water models'; only 2D numerical methods are needed)

Vertical coordinate

- The vertical resolution is implicitly set during `./create_newcase` depending on (physics) configuration. For example, `klev=26` for CAM4, `klev=30` for CAM5 and `klev=32` for CAM6.
- The vertical resolution can be changed with

```
./xmlchange CAM_CONFIG_OPTS=-nlev 30
```

- If horizontal or vertical resolution is changed the user must point to an initial condition file matching that resolution. Non-default initial condition file is set in CAM namelist (`user_nl_cam` located in the *case* directory):

```
ncdata='inputdata/atm/cam/inic/fv/cami-mam3_0000-01-01_0.9x1.25_L30_c100618.nc'
```

- Changing vertical or horizontal resolution requires a 're-compile'.
- WARNING! CAM physics parameterizations are sensitive to resolution (especially vertical resolution) - usually a retuning of parameters is necessary to get an 'acceptable' climate.
- More details on vertical remapping in the Appendix.

Vertical coordinate

The vertical extent is from the surface to

- approximately ∼42 km's / 2Pa for CAM
- approximately ∼140 km's / 10^{-6} hPa for WACCM (Whole Atmosphere Community Climate Model)
- approximately ∼600 km's / 10^{-9} hPa for WACCM-x

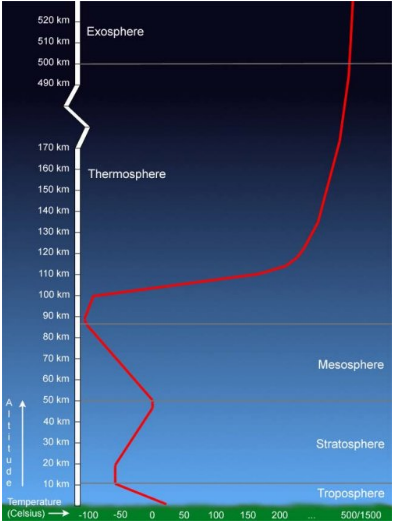

The story so far

We have discussed

- discretization in terms of resolved and un-resolved scales,
- time-space scale overview of phenomena in the atmosphere.
- horizontal and vertical grids,

Now let's dive into the dynamical core:

- what equations of motion should we use and what is the associated thermodynamics?
- what approximations/assumptions are typically made?

Adiabatic frictionless equations of motion

The following dynamic/geometric approximations are made to the compressible Euler equations:

- **spherical geoid**: geopotential Φ is only a function of radial distance from the center of the Earth r: $\Phi = \Phi(r)$ (for planet Earth the true gravitational acceleration is much stronger than the centrifugal force).
  $\Rightarrow$ Effective gravity acts only in radial direction
- **quasi-hydrostatic approximation** (also simply referred to as *hydrostatic approximation*): Involves ignoring the acceleration term in the vertical component of the momentum equations so that it reads:

$$\rho\, g = -\frac{\partial p}{\partial z}, \tag{1}$$

  where g gravity, ρ density and p pressure. Good approximation down to horizontal scales greater than approximately $10km$.
- **shallow atmosphere**: a collection of approximations. Coriolis terms involving the horizontal components of Ω are neglected (Ω is angular velocity), factors $1/r$ are replaced with $1/a$ where a is the mean radius of the Earth and certain other metric terms are neglected so that the system retains **conservation laws for energy and angular momentum**.

Several global dynamical cores no longer make the hydrostatic (e.g. MPAS) and/or shallow atmosphere assumption!

Moist air is considered a mixture of dry air and various forms of water:

Water in the atmosphere

1. **Water vapor (gaseous phase of water): weight of water vapor in the atmosphere corresponds to approximately ~2.4hPa**

2. **Liquid water (clouds): condensation of water vapor form droplets**

3. **Frozen water / ice (clouds): ice crystals**

Cirrus clouds (high clouds)

High resolution models also transport graubel, hail, snow, ...

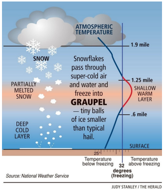

The set of all components of moist air are referred to as:

$$\mathcal{L}_{all} \equiv \{d, wv, cl, ci, rn, sw, gr\}. \quad (2)$$

Note that dry air and water vapor are gases and $'cl'$, $'ci'$, $'rn'$, $'sw'$ and $'gr'$ are condensates (very different thermodynamic properties!)

Adiabatic frictionless equations of motion: thermodynamics and water

Large-scale models (e.g. CAM) assume that:

- the specific volume of condensates (liquid water and ice) is zero, (good approx.)
- moist air is an ideal perfect gas (good approx.):

$$p = \rho^{(all)} R^{(d)} T_v, \tag{3}$$

where p is pressure, $\rho^{(all)}$ is the density of moist air, $R^{(d)}$ the gas constant for dry air and T_v virtual temperature

$$T_v = T \left(\frac{1 + \frac{R^{(wv)}}{R^{(d)}} m^{(wv)}}{\sum_{\ell \in \mathcal{L}_{all}} m^{(\ell)}} \right) \simeq T \left(\frac{1 + \frac{R^{(wv)}}{R^{(d)}} m^{(wv)}}{1 + m^{(wv)}} \right) = T \left[1 + \left(\frac{R^{(wv)}}{R^{(d)}} - 1 \right) q^{(wv)} \right] \tag{4}$$

- specific heats are constants independent of temperature (good approx.),
- single temperature assumption, i.e. no separate thermodynamic equation for condensates (questionable? - gets complicated but doable; Bannon, 2002),
- single velocity assumption, i.e. no separate momentum equations for condensates (questionable?).

Note: it is easy to lose thermodynamic consistency if approximations are made to thermodynamic expressions individually (e.g. (4))→ violations of the first and/or second laws of thermodynamics, Solution: use thermodynamic potentials from which all thermodynamics variables (p, enthalpy, etc,) can be derived (see, e.g., Bowen and Thuburn, 2022a,b).

Adiabatic frictionless equations of motion: thermodynamics and water

Large-scale models (e.g. CAM) assume that:

- the specific volume of condensates (liquid water and ice) is zero, (good approx.)
- moist air is an ideal perfect gas (good approx.):

$$p = \rho^{(all)} R^{(d)} T_v, \tag{3}$$

  where p is pressure, $\rho^{(all)}$ is the density of moist air, $R^{(d)}$ the gas constant for dry air and T_v virtual temperature

$$T_v = T\left(\frac{1+\frac{R^{(wv)}}{R^{(d)}}m^{(wv)}}{\sum_{\ell\in\mathcal{L}_{all}} m^{(\ell)}}\right) \simeq T\left(\frac{1+\frac{R^{(wv)}}{R^{(d)}}m^{(wv)}}{1+m^{(wv)}}\right) = T\left[1+\left(\frac{R^{(wv)}}{R^{(d)}}-1\right)q^{(wv)}\right] \tag{4}$$

- specific heats are constants independent of temperature (good approx.),
- single temperature assumption, i.e. no separate thermodynamic equation for condensates (questionable? - gets complicated but doable; Bannon, 2002),
- single velocity assumption, i.e. no separate momentum equations for condensates (questionable?).

Closed total energy budgets are important in coupled climate modeling and is quite complicated - for a 'pedagogical' introduction to this subject see, e.g., Lauritzen et al. (2022). [warning: $\sim$ 100 pages]

Adiabatic frictionless equations of motion using Lagrangian vertical coordinates

Assuming a Lagrangian vertical coordinate the hydrostatic equations of motion integrated over a layer can be written as

$$\begin{aligned}
\text{mass air:} \quad & \frac{\partial(\delta p)}{\partial t} = -\nabla_h \cdot (\vec{v}_h \delta p)\,, \\
\text{mass tracers:} \quad & \frac{\partial(\delta p q^{(\ell)})}{\partial t} = -\nabla_h \cdot \left(\vec{v}_h\, q^{(\ell)} \delta p\right)\,, \quad \ell \in \mathcal{L}_{all} \\
\text{horizontal momentum:} \quad & \frac{\partial \vec{v}_h}{\partial t} = -\left(\zeta + f\right) \vec{k} \times \vec{v}_h - \nabla_h \kappa - \nabla_p \Phi, \\
\text{thermodynamic:} \quad & \frac{\partial(\delta p \Theta)}{\partial t} = -\nabla_h \cdot (\vec{v}_h \delta p \Theta)
\end{aligned}$$

where δp is the layer thickness, $\vec{v}_h$ is horizontal wind, q tracer mixing ratio, ζ vorticity, f Coriolis, κ kinetic energy, Θ potential temperature. The momentum equations are written in vector invariant form.

Adiabatic frictionless equations of motion using Lagrangian vertical coordinates

Assuming a Lagrangian vertical coordinate the hydrostatic equations of motion integrated over a layer can be written as

$$\begin{aligned}
\text{mass air:} \quad & \frac{\partial(\delta p)}{\partial t} = -\nabla_h \cdot \left(\vec{v}_h \delta p\right), \\
\text{mass tracers:} \quad & \frac{\partial(\delta p q^{(\ell)})}{\partial t} = -\nabla_h \cdot \left(\vec{v}_h \, q^{(\ell)} \delta p\right), \quad \ell \in \mathcal{L}_{all} \\
\text{horizontal momentum:} \quad & \frac{\partial \vec{v}_h}{\partial t} = -\left(\zeta + f\right) \vec{k} \times \vec{v}_h - \nabla_h \kappa - \nabla_p \Phi, \\
\text{thermodynamic:} \quad & \frac{\partial(\delta p \Theta)}{\partial t} = -\nabla_h \cdot \left(\vec{v}_h \delta p \Theta\right)
\end{aligned}$$

The equations of motion are discretized using an Eulerian finite-volume approach.

Finite-volume discretization of continuity equation

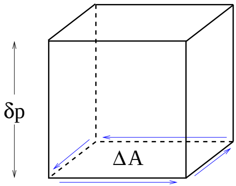

Integrate the flux-form continuity equation horizontally over a control volume:

$$\frac{\partial}{\partial t} \iint_A \delta p \, dA = - \iint_A \nabla_h \left(\vec{v}_h \delta p \right) \, dA, \tag{5}$$

where A is the horizontal extent of the control volume. Using Gauss's divergence theorem for the right-hand side of (5) we get:

$$\frac{\partial}{\partial t} \iint_A \delta p \, dA = - \oint_{\partial A} \delta p \, \vec{v} \cdot \vec{n} \, dA, \tag{6}$$

where ∂A is the boundary of A and $\vec{n}$ is outward pointing normal unit vector of ∂A.

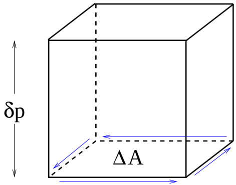

Integrate the flux-form continuity equation horizontally over a control volume:

$$\frac{\partial}{\partial t}\iint_A \delta p \, dA = -\iint_A \nabla_h \left(\vec{v}_h \delta p\right) \, dA, \tag{5}$$

where A is the horizontal extent of the control volume. Using Gauss's divergence theorem for the right-hand side of (5) we get:

$$\frac{\partial}{\partial t}\iint_A \delta p \, dA = -\oint_{\partial A} \delta p \, \vec{v} \cdot \vec{n} \, dA, \tag{6}$$

Right-hand side of (6) represents the instantaneous flux of mass through the vertical faces of the control volume.

Next: integrate over one time-step Δt_{dyn} and discretize left-hand side.

Finite-volume discretization of continuity equation

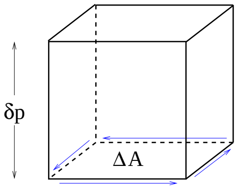

Integrate the flux-form continuity equation horizontally over a control volume:

$$\frac{\partial}{\partial t}\iint_A \delta p \, dA = -\iint_A \nabla_h \left(\vec{v}_h \delta p\right) \, dA, \tag{5}$$

$$\Delta A \, \overline{\delta p}^{n+1} - \Delta A \, \overline{\delta p}^{n} = -\Delta t_{dyn} \int_{t=n\Delta t}^{t=(n+1)\Delta t} \left[\oint_{\partial A} \delta p \, \vec{v} \cdot \vec{n} \, dA \right] dt, \tag{6}$$

where n is time-level index and $\overline{(\cdot)}$ is cell-averaged value.

The right-hand side represents the mass transported through all of the four vertical control volume faces into the cell during one time-step. Graphical illustration on next slide!

Finite-volume discretization of continuity equation: Tracking mass

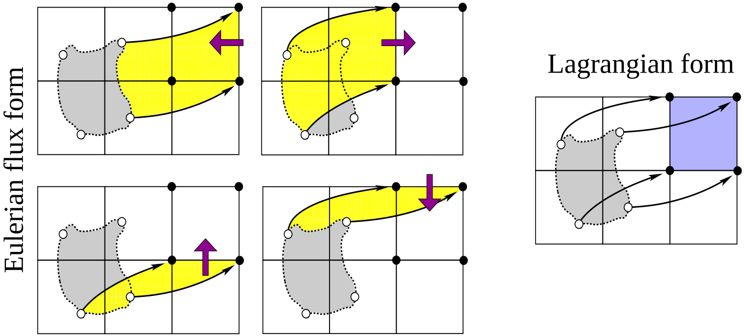

The yellow areas are 'swept' through the control volume faces during one time-step. The grey area is the corresponding Lagrangian area (area moving with the flow with no flow through its boundaries that ends up at the Eulerian control volume after one time-step). Black arrows show parcel trajectories.

Note **equivalence** between Eulerian flux-form and Lagrangian form!

(Lauritzen et al., 2011b)

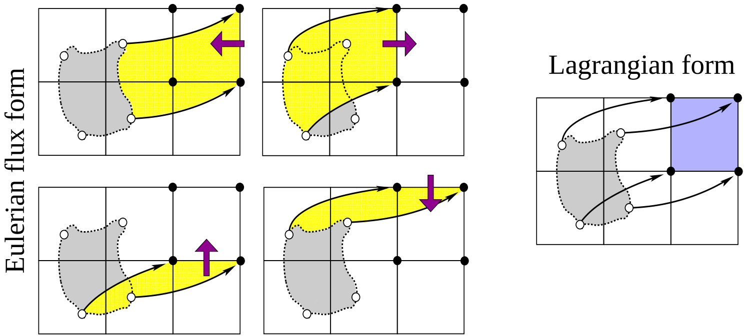

Until now everything has been exact. How do we approximate the fluxes numerically?

- In CAM-FV the Lin and Rood (1996) scheme is used which is a dimensionally split scheme (that is, rather than 'explicitly' estimating the boundaries of the yellow areas and integrate over them, fluxes are estimated by successive applications of one-dimensional operators in each coordinate direction).

The Lin and Rood (1996) advection scheme

$$\overline{\delta p}^{n+1} = \overline{\delta p}^{n} + F^{\lambda}\left[\frac{1}{2}\left(\overline{\delta p}^{n} + f^{\theta}(\overline{\delta p}^{n})\right)\right] + F^{\theta}\left[\frac{1}{2}\left(\overline{\delta p}^{n} + f^{\lambda}(\overline{\delta p}^{n})\right)\right],$$

where

$$F^{\lambda,\theta} = \text{ flux divergence in } \lambda \text{ or } \theta \text{ coordinate direction}$$
$$f^{\lambda,\theta} = \text{ advective update in } \lambda \text{ or } \theta \text{ coordinate direction}$$

The Lin and Rood (1996) advection scheme

$$\overline{\delta p}^{n+1} = \overline{\delta p}^{n} + F^{\lambda}\left[\frac{1}{2}\left(\overline{\delta p}^{n} + f^{\theta}(\overline{\delta p}^{n})\right)\right] + F^{\theta}\left[\frac{1}{2}\left(\overline{\delta p}^{n} + f^{\lambda}(\overline{\delta p}^{n})\right)\right],$$

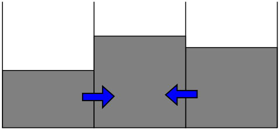

- Figure: Graphical illustration of flux-divergence operator F^{λ}. Shaded areas show cell average values for the cell we wish to make a forecast for and the two adjacent cells.

The Lin and Rood (1996) advection scheme

$$\overline{\delta p}^{n+1} = \overline{\delta p}^{n} + F^{\lambda}\left[\frac{1}{2}\left(\overline{\delta p}^{n} + f^{\theta}(\overline{\delta p}^{n})\right)\right] + F^{\theta}\left[\frac{1}{2}\left(\overline{\delta p}^{n} + f^{\lambda}(\overline{\delta p}^{n})\right)\right],$$

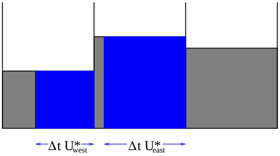

- $u^{*}_{East/West}$ are the time-averaged winds on each face (more on how these are obtained later).
- F^{λ} is proportional to the difference between mass 'swept' through East and West cell face.
- $f^{\lambda} = F^{\lambda} + \overline{\overline{<\delta p>}}\Delta t_{dyn} D$, where D is divergence.
- On Figure we assume constant sub-grid-cell reconstructions for the fluxes.

The Lin and Rood (1996) advection scheme

$$\overline{\delta p}^{n+1} = \overline{\delta p}^{n} + F^{\lambda}\left[\frac{1}{2}\left(\overline{\delta p}^{n} + f^{\theta}(\overline{\delta p}^{n})\right)\right] + F^{\theta}\left[\frac{1}{2}\left(\overline{\delta p}^{n} + f^{\lambda}(\overline{\delta p}^{n})\right)\right],$$

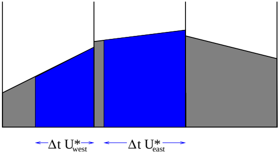

Higher-order approximation to the fluxes:

- Piecewise linear sub-grid-scale reconstruction (van Leer, 1977): Fit a linear function using neighboring grid-cell average values with mass-conservation as a constraint (i.e. area under linear function = cell average).

The Lin and Rood (1996) advection scheme

$$\overline{\delta p}^{n+1} = \overline{\delta p}^{n} + F^{\lambda}\left[\frac{1}{2}\left(\overline{\delta p}^{n} + f^{\theta}(\overline{\delta p}^{n})\right)\right] + F^{\theta}\left[\frac{1}{2}\left(\overline{\delta p}^{n} + f^{\lambda}(\overline{\delta p}^{n})\right)\right],$$

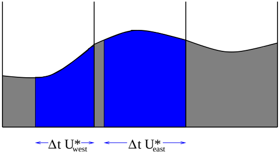

Higher-order approximation to the fluxes:

- Piecewise linear sub-grid-scale reconstruction (van Leer, 1977): Fit a linear function using neighboring grid-cell average values with mass-conservation as a constraint (i.e. area under linear function = cell average).
- Piecewise parabolic sub-grid-scale reconstruction (Colella and Woodward, 1984): Fit parabola using neighboring grid-cell average values with mass-conservation as a constraint. Note: Reconstruction is C^0 across cell edges.

The Lin and Rood (1996) advection scheme

$$\overline{\delta p}^{n+1} = \overline{\delta p}^{n} + F^{\lambda}\left[\frac{1}{2}\left(\overline{\delta p}^{n} + f^{\theta}(\overline{\delta p}^{n})\right)\right] + F^{\theta}\left[\frac{1}{2}\left(\overline{\delta p}^{n} + f^{\lambda}(\overline{\delta p}^{n})\right)\right],$$

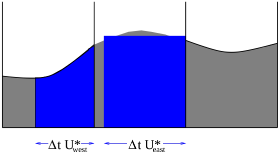

Higher-order approximation to the fluxes:

- Piecewise linear sub-grid-scale reconstruction (van Leer, 1977): fit a linear function using neighboring grid-cell average values with mass-conservation as a constraint (i.e. area under linear function = cell average).
- Piecewise parabolic sub-grid-scale reconstruction (Colella and Woodward, 1984): fit parabola using neighboring grid-cell average values with mass-conservation as a constraint. Note: reconstruction is continuous at cell edges.
- Reconstruction function may 'overshoot' or 'undershoot' which may lead to unphysical and/or oscillatory solutions. Use limiters to render reconstruction function shape-preserving.

The Lin and Rood (1996) advection scheme

$$\overline{\delta p}^{n+1} = \overline{\delta p}^{n} + F^{\lambda}\left[\frac{1}{2}\left(\overline{\delta p}^{n} + f^{\theta}(\overline{\delta p}^{n})\right)\right] + F^{\theta}\left[\frac{1}{2}\left(\overline{\delta p}^{n} + f^{\lambda}(\overline{\delta p}^{n})\right)\right],$$

Advantages:

- Inherently mass conservative (note: conservation does not necessarily imply accuracy!).
- Formulated in terms of one-dimensional operators.
- Preserves constant mass field for a non-divergent flow field (if the finite-difference approximation to divergence is zero).
- Preserves linear correlations between trace species (if shape-preservation filters are not applied)
- Has shape-preserving options.
- CAM-FV uses the PPM (Piecewise Parabolic Method; Colella and Woodward, 1984) with shape-preserving filters described in Lin and Rood (1996)

Namelist variables for *outer* operators

- In top layers operators are reduced to first order:

  if (`k`$\leq$`klev/8`) `IORD=JORD=1`

  E.g., for `klev=30` the operators are altered in the top 3 layers.

- The advective $f^{\lambda,\theta}$ (*inner*) operators are 'hard-coded' to 1st order. For a linear analysis of the consequences of using *inner* and *outer* operators of different orders see Lauritzen (2007).

Adiabatic frictionless equations of motion

Hydrostatic equations of motion integrated over a Lagrangian layer

$$
\begin{aligned}
\frac{\partial(\delta p)}{\partial t} &= -\nabla_h \cdot (\vec{v}_h \delta p)\,, \\
\frac{\partial(\delta p q^{(\ell)})}{\partial t} &= -\nabla_h \cdot (\vec{v}_h \delta p)\,, \\
\frac{\partial \vec{v}_h}{\partial t} &= -\left(\zeta + f\right) \vec{k} \times \vec{v}_h - \nabla_h \kappa - \nabla_p \Phi, \\
\frac{\partial(\delta p \Theta)}{\partial t} &= -\nabla_h \cdot (\vec{v}_h \delta p \Theta)
\end{aligned}
$$

The equations of motion are discretized using an Eulerian finite-volume approach.

Hydrostatic equations of motion integrated over a Lagrangian layer

$$
\begin{aligned}
\overline{\delta p}^{n+1} &= \overline{\delta p}^{n} + F^{\lambda}\left[\frac{1}{2}\left(\overline{\delta p}^{n} + f^{\theta}(\overline{\delta p}^{n})\right)\right] + F^{\theta}\left[\frac{1}{2}\left(\overline{\delta p}^{n} + f^{\lambda}(\overline{\delta p}^{n})\right)\right], \\
\frac{\partial(\delta p q^{(\ell)})}{\partial t} &= -\nabla_h \cdot \left(\vec{v}_h \delta p\right), \\
\frac{\partial \vec{v}_h}{\partial t} &= -\left(\zeta + f\right)\vec{k} \times \vec{v}_h - \nabla_h \kappa - \nabla_p \Phi, \\
\frac{\partial(\delta p \Theta)}{\partial t} &= -\nabla_h \cdot \left(\vec{v}_h \delta p \Theta\right)
\end{aligned}
$$

Adiabatic frictionless equations of motion

Hydrostatic equations of motion integrated over a Lagrangian layer

$$
\begin{aligned}
\overline{\delta p}^{n+1} &= \overline{\delta p}^{n} + F^{\lambda}\left[\frac{1}{2}\left(\overline{\delta p}^{n} + f^{\theta}(\overline{\delta p}^{n})\right)\right] + F^{\theta}\left[\frac{1}{2}\left(\overline{\delta p}^{n} + f^{\lambda}(\overline{\delta p}^{n})\right)\right], \\
\overline{\delta p q^{(\ell)}}^{n+1} &= \text{super-cycled (details in Appendix)}, \\
\frac{\partial \vec{v}_h}{\partial t} &= -\left(\zeta + f\right)\vec{k} \times \vec{v}_h - \nabla_h \kappa - \nabla_p \Phi, \\
\frac{\partial(\delta p \Theta)}{\partial t} &= -\nabla_h \cdot \left(\vec{v}_h \delta p \Theta\right)
\end{aligned}
$$

Adiabatic frictionless equations of motion

Hydrostatic equations of motion integrated over a Lagrangian layer

$$
\begin{aligned}
\overline{\delta p}^{n+1} &= \overline{\delta p}^{n} + F^{\lambda}\left[\frac{1}{2}\left(\overline{\delta p}^{n} + f^{\theta}(\overline{\delta p}^{n})\right)\right] + F^{\theta}\left[\frac{1}{2}\left(\overline{\delta p}^{n} + f^{\lambda}(\overline{\delta p}^{n})\right)\right], \\
\overline{\delta p q^{(\ell)}}^{n+1} &= \text{super-cycled (details in Appendix)}, \\
\vec{v}_h^{n+1} &= \vec{v}_h^{n} - \vec{\Gamma}^1\left[(\zeta + f)\,\vec{k} \times \vec{v}_h\right] - \nabla_h\left(\vec{\Gamma}^2 \kappa\right) - \Delta t_{dyn}\widehat{P}, \\
\frac{\partial(\delta p \Theta)}{\partial t} &= -\nabla_h \cdot (\vec{v}_h \delta p \Theta)
\end{aligned}
$$

- $\vec{\Gamma}^1$ is operator using combinations of $F^{\lambda,\theta}$ and $f^{\lambda,\theta}$ as components to approximate the time-volume-average of the vertical component of absolute vorticity. Similarly for $\vec{\Gamma}^2$ but for kinetic energy. ∇_h is simply approximated by finite differences. For details see Lin (2004).
- $\widehat{P}$ is a finite-volume discretization of the pressure gradient force (see Lin 1997 for details).

Adiabatic frictionless equations of motion

Hydrostatic equations of motion integrated over a Lagrangian layer

$$
\begin{aligned}
\overline{\delta p}^{n+1} &= \overline{\delta p}^{n} + F^{\lambda}\left[\frac{1}{2}\left(\overline{\delta p}^{n} + f^{\theta}(\overline{\delta p}^{n})\right)\right] + F^{\theta}\left[\frac{1}{2}\left(\overline{\delta p}^{n} + f^{\lambda}(\overline{\delta p}^{n})\right)\right], \\
\overline{\delta p q^{(\ell)}}^{n+1} &= \text{super-cycled (details in Appendix)}, \\
\vec{v}_h^{n+1} &= \vec{v}_h^{n} - \vec{\Gamma}^{1}\left[(\zeta + f)\,\vec{k} \times \vec{v}_h\right] - \nabla_h\left(\vec{\Gamma}^{2}\kappa\right) - \Delta t_{dyn}\widehat{P}, \\
\overline{\Theta\delta p}^{n+1} &= \overline{\Theta\delta p}^{n} + F^{\lambda}\left[\frac{1}{2}\left(\overline{\Theta\delta p}^{n} + f^{\theta}(\overline{\Theta\delta p}^{n})\right)\right] + F^{\theta}\left[\frac{1}{2}\left(\overline{\Theta\delta p}^{n} + f^{\lambda}(\overline{\Theta\delta p}^{n})\right)\right],
\end{aligned}
$$

Adiabatic frictionless equations of motion

Hydrostatic equations of motion integrated over a Lagrangian layer

$$\overline{\delta p}^{n+1} = \overline{\delta p}^{n} + F^{\lambda}\left[\frac{1}{2}\left(\overline{\delta p}^{n} + f^{\theta}(\overline{\delta p}^{n})\right)\right] + F^{\theta}\left[\frac{1}{2}\left(\overline{\delta p}^{n} + f^{\lambda}(\overline{\delta p}^{n})\right)\right],$$

$$\overline{\delta p q^{(\ell)}}^{n+1} = \text{super-cycled (details in Appendix)},$$

$$\vec{v}_h^{n+1} = \vec{v}_h^{n} - \vec{\Gamma}^{1}\left[(\zeta + f)\,\vec{k}\times\vec{v}_h\right] - \nabla_h\left(\vec{\Gamma}^{2}\kappa\right) - \Delta t_{dyn}\widehat{P},$$

$$\overline{\Theta\delta p}^{n+1} = \overline{\Theta\delta p}^{n} + F^{\lambda}\left[\frac{1}{2}\left(\overline{\Theta\delta p}^{n} + f^{\theta}(\overline{\Theta\delta p}^{n})\right)\right] + F^{\theta}\left[\frac{1}{2}\left(\overline{\Theta\delta p}^{n} + f^{\lambda}(\overline{\Theta\delta p}^{n})\right)\right],$$

- No explicit diffusion operators in equations (so far!).
- Implicit diffusion trough shape-preservation constraints in F and f operators.
- CAM-FV has 'control' over vorticity at the grid scale through implicit diffusion in the operators F and f but it does not have explicit control over divergence near the grid scale.

Adiabatic frictionless equations of motion

Hydrostatic equations of motion integrated over a Lagrangian layer

$$\overline{\delta p}^{n+1} = \overline{\delta p}^{n} + F^{\lambda}\left[\frac{1}{2}\left(\overline{\delta p}^{n} + f^{\theta}(\overline{\delta p}^{n})\right)\right] + F^{\theta}\left[\frac{1}{2}\left(\overline{\delta p}^{n} + f^{\lambda}(\overline{\delta p}^{n})\right)\right],$$

$$\overline{\delta p q^{(\ell)}}^{n+1} = \text{super-cycled (details in Appendix)},$$

$$\vec{v}_h^{n+1} = \vec{v}_h^{n} - \vec{\Gamma}^{1}\left[(\zeta + f)\,\vec{k}\times\vec{v}_h\right] - \nabla_h\left(\vec{\Gamma}^{2}\kappa\right) - \Delta t_{dyn}\widehat{P} + \Delta t_{dyn}\nabla_h\left(\nu\nabla_h^{\ell} D\right), \ell = 0, 2$$

$$\overline{\Theta\delta p}^{n+1} = \overline{\Theta\delta p}^{n} + F^{\lambda}\left[\frac{1}{2}\left(\overline{\Theta\delta p}^{n} + f^{\theta}(\overline{\Theta\delta p}^{n})\right)\right] + F^{\theta}\left[\frac{1}{2}\left(\overline{\Theta\delta p}^{n} + f^{\lambda}(\overline{\Theta\delta p}^{n})\right)\right],$$

- No explicit diffusion operators in equations.
- Implicit diffusion trough shape-preservation constraints in F and f operators.
- The above discretization leads to 'control' over vorticity at the grid scale through implicit diffusion but no explicit control over divergence.
- Add divergence damping (2^{nd}-order or 4^{th}-order) term to momentum equations.
  Optionally a 'Laplacian-like' damping of wind components is used in upper 3 levels to slow down excessive polar night jet that appears at high horizontal resolutions.
  namelist variable: `fv_div24del2flag`

More details: Lauritzen et al. (2011a); for a stability analysis of divergence damping in CAM see Whitehead et al. (2011)

Total kinetic energy spectra

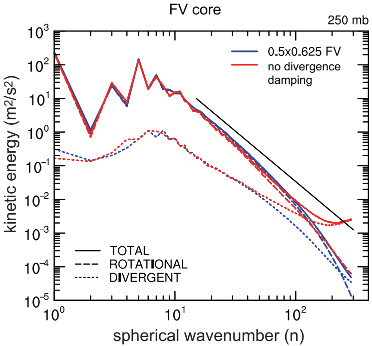

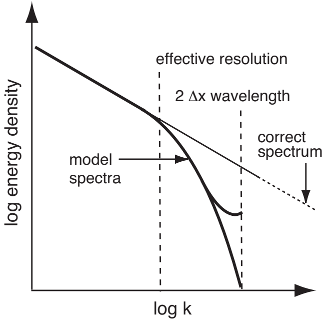

Figure: (left) Solid black line shows k^{-3} slope (courtesy of D.L. Williamson). (right) Schematic of 'effective resolution' (Figure from Skamarock (2011)).

- (left) Without divergence damping there is a spurious accumulation of total kinetic energy associated with divergent modes near the grid scale.
- (right) Note: total kinetic energy spectra can also be used to assess 'effective resolution' (see, e.g., discussion in Skamarock, 2011)

The reformulation of global climate/weather models for massively parallel computer architectures

The reformulation of global climate/weather models for massively parallel computer architectures

Traditionally the equations of motion have been discretized on the traditional regular latitude-longitude grid using either

1. spherical harmonics based methods (dominated for over 40 years)
2. finite-difference/finite-volume methods (e.g., CAM-FV)

Both methods require non-local communication:

1. Legendre transform
2. 'polar[a] filters' (due to convergence of the meridians near the poles)

respectively, and are therefore not "trivially" amenable for massively parallel compute systems.

[a] confusing terminology: filters are also applied away from polar regions: $\theta \in [\pm 36^\circ, \pm 90]$

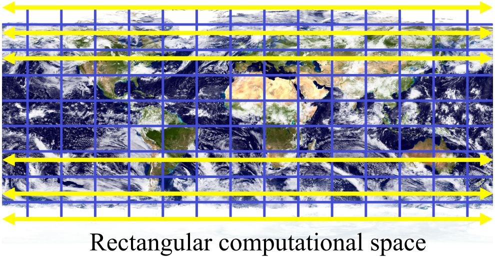

The reformulation of global climate/weather models for massively parallel computer architectures

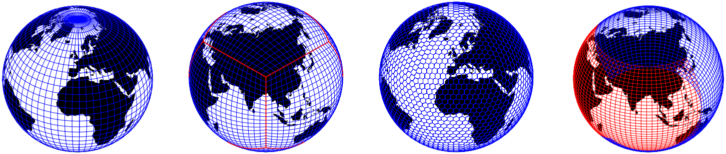

- Quasi-uniform grid + local numerical method ⇒ no non-local communication necessary

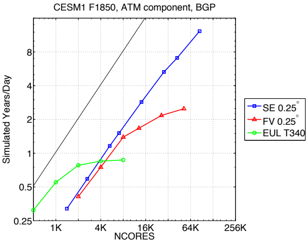

Performance in through-put for different dynamical cores in NCAR's global atmospheric climate model:

horizontal resolution: approximately 25km × 25km grid boxes

- EUL = spectral transform (lat-lon grid)
- FV = finite-volume (reg. lat-lon grid)
- SE = spectral element (cubed-sphere grid)

Computer = Intrepid (IBM Blue Gene/P Solution) at Argonne National Laboratory

Note that for small compute systems CAM-EUL has SUPERIOR throughput!!

Scalable dynamical cores in CAM

- CAM-SE (Lauritzen et al., 2018): Spectral Elements
  - Dynamical core based on HOMME (High-Order Method Modeling Environment, Thomas and Loft 2005).
  - Mass-conservative to machine precision and good total energy conservation properties
  - Conserves axial angular momentum very well (Lauritzen et al., 2014)
  - Discretized on cubed-sphere (uniform resolution or conforming mesh-refinement; Zarzycki et al., 2014) and highly scalable
  - 'Work-horse' for high resolution climate applications ($1/4^\circ$) and planned 'work-horse' for 1° climate applications
  - New NCAR CAM-SE version using dry-mass vertical coordinates and with comprehensive treatment of condensates and energy released with CESM2
  - Optional transport with finite-volume scheme (Lauritzen et al., 2017) and finite-volume physics grid (Herrington et al., 2018, 2019)

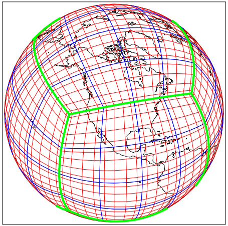

- MPAS (Skamarock et al., 2012): Finite-volume unstructured
  - MPAS = Model for Prediction Across Scales
  - Centroidal Voronoi tessellation of the sphere
  - Fully compressible non-hydrostatic discretization similar to Weather Research Weather (WRF) model (Skamarock and Klemp, 2008)

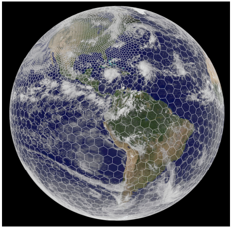

- FV3: Finite-volume
  - 'cubed-sphere' version of CAM-FV (only hydrostatic version supported in CESM; no mesh-refinement supported)
    `https://www.gfdl.noaa.gov/fv3/fv3-documentation-and-references/`

Figures courtesy of R.D. Nair (upper) and W.C. Skamarock (lower).

Functional support for variable resolution mesh configurations with CAM-SE

DO NOT USE CESM2.2 RELEASE OF CAM-SE ... USE `cam_development`

- Recent release of CESM2.2 has support for 3 variable resolution meshes:

Figures courtesy of Adam Herrington

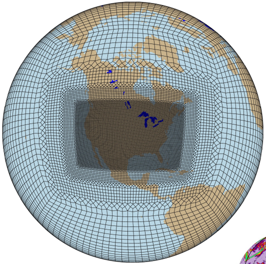

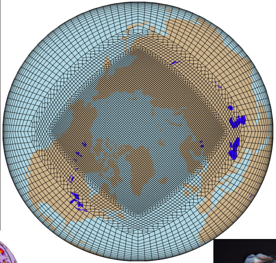

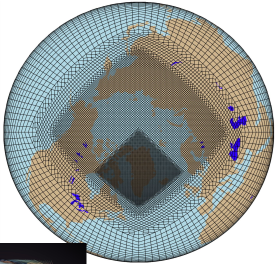

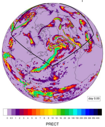

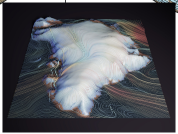

Herrington et al. (2022)

The challenge with variable resolution is well-behaved physics!

DO NOT USE CESM2.2 RELEASE OF CAM-SE ... USE `cam_development`

A success story for variable resolution!

Surface Mass Balance (SMB) Temporal Evolution

SMB = ACCUM* + RUNOFF

*includes meltwater storage/refreezing

- Too much ACCUM at low res
- Too much RUNOFF at low res*

ANN Climo (1979-1998) minus RACMO ANN Climo (1979-1998)

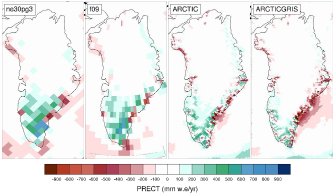

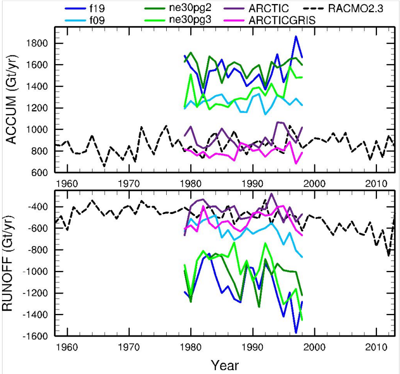

Slide courtesy of Adam Herrington

Herrington et al. (2022)

Functional support for variable resolution mesh configurations with CAM-SE

DO NOT USE CESM2.2 RELEASE OF CAM-SE ... USE `cam_development`

Wanna make your own grids?

`https://github.com/ESMCI/Community_Mesh_Generation_Toolkit/blob/master/VRM_tools/Docs/VRM_Grids_For_CAMSE.pdf`

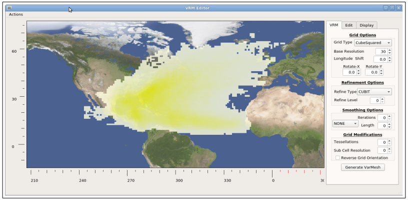

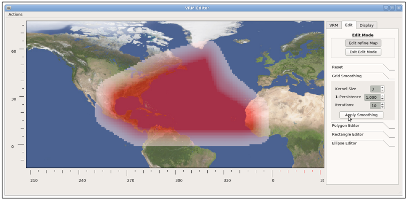

Interested in numerical methods for geophysical fluid dynamics?

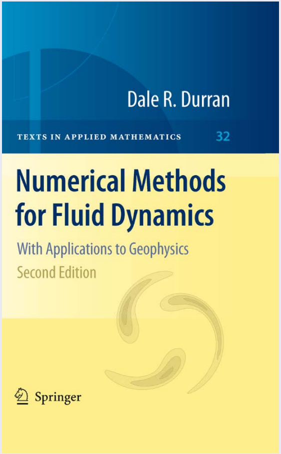

- Numerical Methods for Fluid Dynamics: with Applications in Geophysics (2nd Ed) New York: Springer, ISBN 978-1-4419-6411-3, 516 p.
- Errata: `https://www.atmos.washington.edu/~durrand/book_errata_2nd.pdf`

Interested in numerical methods for global models?

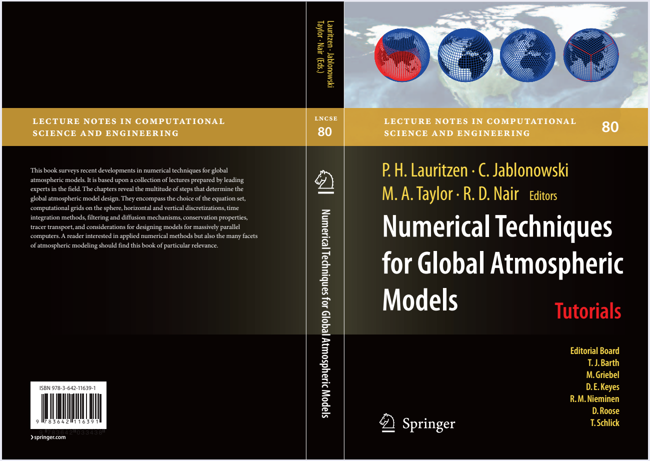

- Book based on the lectures given at the 2008 NCAR ASP (Advance Study Program) Summer Colloquium.
- 16 Chapters; authors include J.Thuburn, J.Tribbia, D.Durran, T.Ringler, W.Skamarock, R.Rood, J.Dennis, Editors, ... Foreword by D. Randall
- More details at: http://www.cgd.ucar.edu/cms/pel/colloquium.html and http://www.cgd.ucar.edu/cms/pel/lncse.html

Questions? Contact pel@ucar.edu

Appendix

CAM-SE: (Lauritzen et al., 2018)

CAM-SE uses a continuous Galerkin finite element method (Taylor et al., 1997) referred to as **Spectral Elements (SE)**:

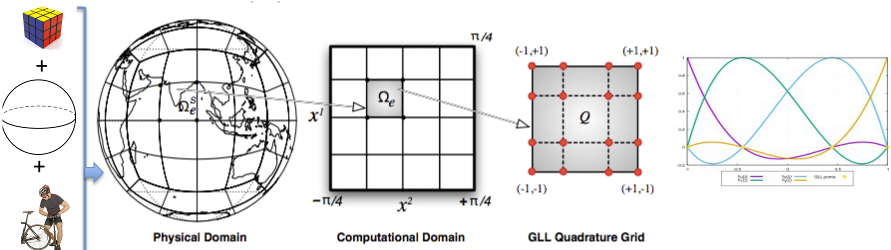

Figures from Nair et al. (2011)

- Physical domain: Tile the sphere with quadrilaterals using the gnomonic cubed-sphere projection
- Computational domain: Mapped local Cartesian domain
- Each element operates with a Gauss-Lobatto-Legendre (GLL) quadrature grid

  Gaussian quadrature using the GLL grid will integrate a polynomial of degree $2N-1$ exactly, where N is degree of polynomial
- Elementwise the solution is projected onto a tensor product of 1D Legendre basis functions

  by multiplying the equations of motion by test functions; *weak Galerkin formation*

  $\rightarrow$ all derivatives inside each element can be computed analytically!

CAM-SE: (Lauritzen et al., 2018)

CAM-SE uses a continuous Galerkin finite element method (Taylor et al., 1997) referred to as **Spectral Elements (SE)**:

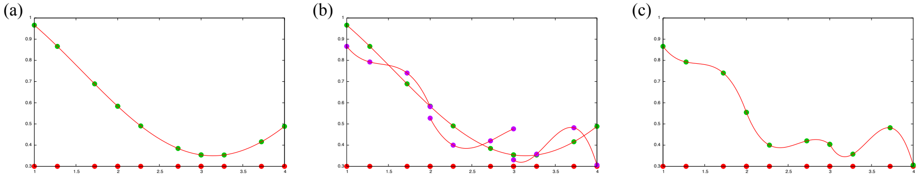

How do solutions in each element 'communicate' with each other?

- The solution is projected onto the space of globally continuous (C^0) piecewise polynomials
- $\rightarrow$ point values are forced to be C^0 continuous along element boundaries by averaging.
- Note: this is the only operation in which information 'propagates' between elements
- MPI data-communication: only information on the boundary of elements!
- For more details see explanation/discussion in Herrington et al. (2018).

Free-stream preserving 'super-cycling' of tracers with respect to air ρ

Simply solving the tracer continuity equation for $\overline{q^{(\ell)}\delta p}^{n+1}$ using Δt_{trac} will lead to inconsistencies. Why?

Continuity equation for air δp

$$\frac{\partial \delta p}{\partial t} + \nabla \cdot (\delta p \, \vec{v}_h) = 0, \qquad (7)$$

and a tracer with mixing ratio q

$$\frac{\partial (\delta p \, q)}{\partial t} + \nabla \cdot (\delta p \, q \, \vec{v}_h) = 0, \qquad (8)$$

For $q = 1$ equation (8) reduces to (7). If this is satisfied in the numerical discretizations, the scheme is 'free-stream' preserving.

Solving (8) with $q = 1$ using Δt_{trac} will NOT produce the same solution as solving (7) `nsplit` times using Δt_{dyn}!

Graphical illustration of ‘free stream’ preserving transport of tracers

Assume no flux through East cell wall.

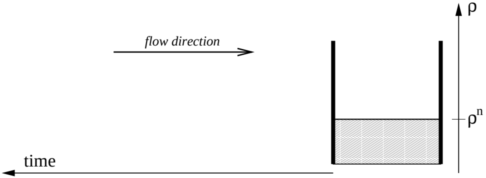

- Solve continuity equation for air δp together with momentum and thermodynamics equations.

Graphical illustration of ‘free stream’ preserving transport of tracers

Assume no flux through East cell wall.

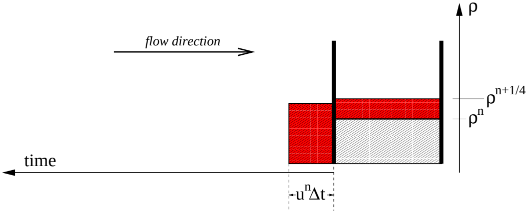

- Solve continuity equation for air δp together with momentum and thermodynamics equations.

Graphical illustration of 'free stream' preserving transport of tracers

Assume no flux through East cell wall.

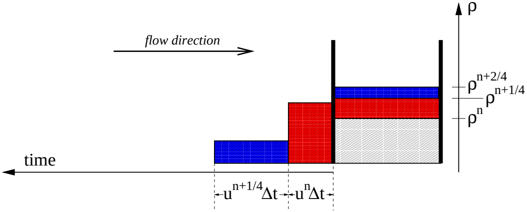

- Solve continuity equation for air δp together with momentum and thermodynamics equations.
- Repeat *nsplit* times

Graphical illustration of ‘free stream’ preserving transport of tracers

Assume no flux through East cell wall.

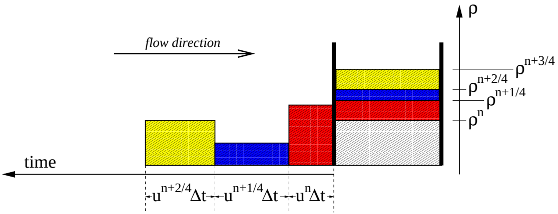

- Solve continuity equation for air δp together with momentum and thermodynamics equations.
- Repeat *nsplit* times

Graphical illustration of 'free stream' preserving transport of tracers

Assume no flux through East cell wall.

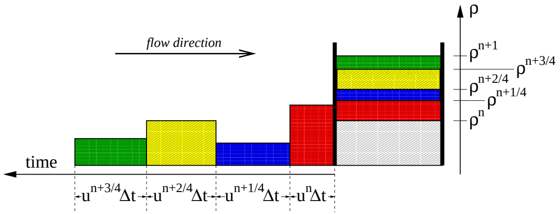

- Solve continuity equation for air δp together with momentum and thermodynamics equations.
- Repeat *nsplit* times

Graphical illustration of 'free stream' preserving transport of tracers

Assume no flux through East cell wall.

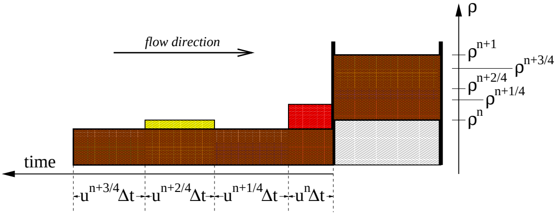

- Solve continuity equation for air δp together with momentum and thermodynamics equations.
- Repeat *nsplit* times
- Brown area = average flow of mass through cell face.
- Compute time-averaged value of q across brown area using Lin and Rood (1996) scheme: $\overline{\overline{<q>}}$.
- Forecast for tracer is: $\overline{\overline{<q>}} \times \sum_{i=1}^{nsplit} \delta p^{n+i/nsplit}$
- Yields 'free stream' preserving solution!

Time-stepping: the 'CD'- grid approach

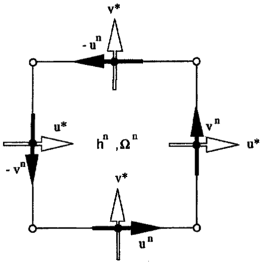

Figure from Lin and Rood (1997).

Definition of Arakawa C and D horizontal staggering (Arakawa and Lamb, 1977):

- C: velocity components at the center of cell faces and orthogonal to cell faces and mass variables at the cell center. Natural choice for mass-flux computations when using Lin and Rood (1996) scheme.
- D: velocity components parallel to cell faces and mass variables at the cell center. Natural choice for computing the circulation of vorticity ($\frac{\partial v}{\partial x} - \frac{\partial u}{\partial y}$).

Time-stepping: the 'CD'- grid approach

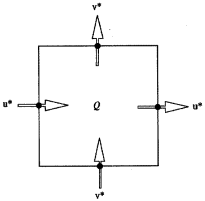

Figure from Lin and Rood (1997).

- For the flux- and advection operators (F and f, respectively) in the Lin and Rood (1996) scheme the time-centered advective winds (u^*, v^*) for the cell faces are needed:
- An option: extrapolate winds (as in semi-Lagrangian models) $\Rightarrow$ can result in noise near steep topography (Lin and Rood, 1997).

- Instead, the equations of motion are integrated forward in time for $\frac{1}{2}\Delta t_{dyn}$ using a C grid horizontal staggering.
- These C-grid winds (u^*, v^*) are then used for the 'full' time-step update (everything else from the C-grid forecast is 'thrown away').
- The 'full' time-step update is performed on a D-grid.
- For a linear stability analysis of the 'CD'-grid approach see Skamarock (2008).

Aside: hybrid sigma ($\sigma = p/p_s$)-pressure (p) coordinate

While terrain-following coordinates simplify the bottom boundary condition, they may introduce errors:

- Pressure gradient force (PDF) errors: $\frac{1}{\rho}\nabla p_z = \frac{1}{\rho}\nabla_\eta p + \frac{1}{\rho}\frac{dp}{dz}\nabla_\eta z$, (Kasahara, 1974) where ρ is density, p pressure and z height.
- Errors in modeling flow along constant z-surfaces near the surface

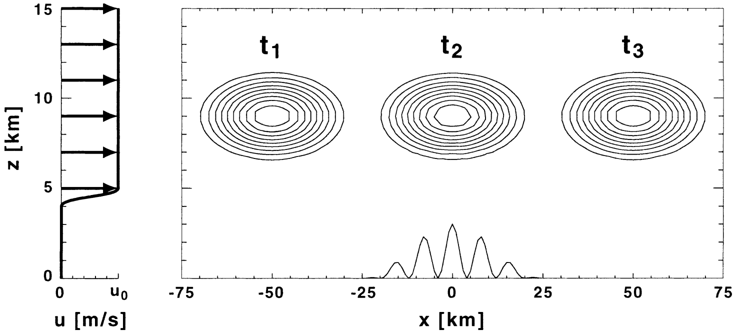

FIG. 4. Vertical cross section of the idealized two-dimensional advection test. The topography is located entirely within a stagnant pool of air, while there is a uniform horizontal velocity aloft. The analytical solution of the advected anomaly is shown at three instances.

Schär et al. (2002)

Aside: hybrid sigma ($\sigma = p/p_s$)-pressure (p) coordinate

While terrain-following coordinates simplify the bottom boundary condition, they may introduce errors:

- Pressure gradient force (PDF) errors: $\frac{1}{\rho}\nabla p_z = \frac{1}{\rho}\nabla_\eta p + \frac{1}{\rho}\frac{dp}{dz}\nabla_\eta z$, (Kasahara, 1974) where ρ is density, p pressure and z height.
- Errors in modeling flow along constant z-surfaces near the surface

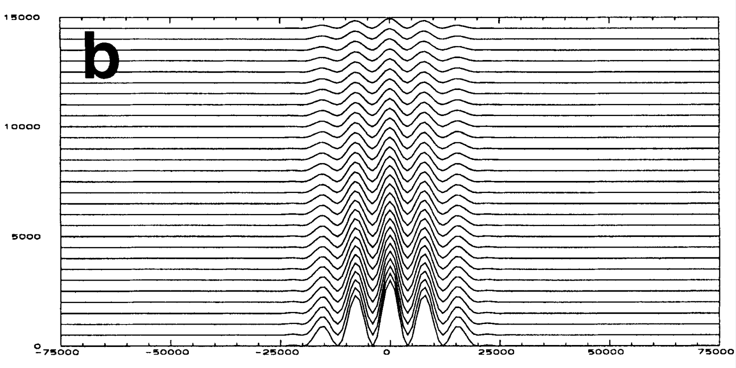

Schär et al. (2002)

While terrain-following coordinates simplify the bottom boundary condition, they may introduce errors:

- Pressure gradient force (PDF) errors: $\frac{1}{\rho}\nabla p_z = \frac{1}{\rho}\nabla_\eta p + \frac{1}{\rho}\frac{dp}{dz}\nabla_\eta z$, (Kasahara, 1974) where ρ is density, p pressure and z height.
- Errors in modeling flow along constant z-surfaces near the surface

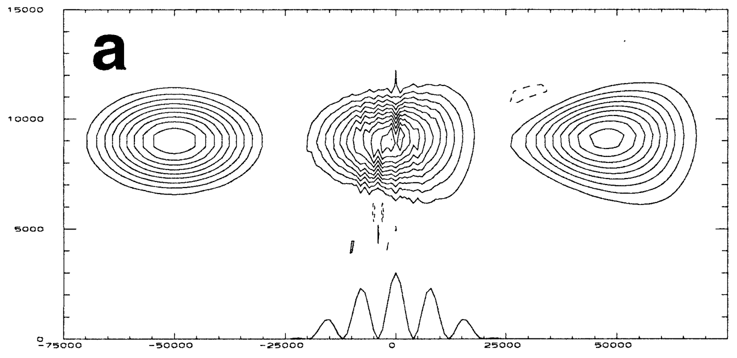

Schär et al. (2002)

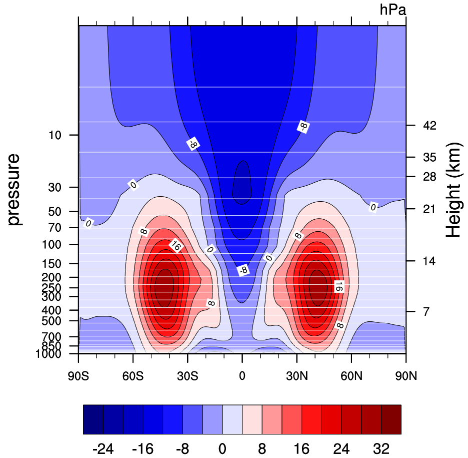

Time & zonally averaged zonal wind (Held-Suarez forcing); overlaid CAM5 levels ($klev = 30$).

Why do we use terrain-following coordinates?

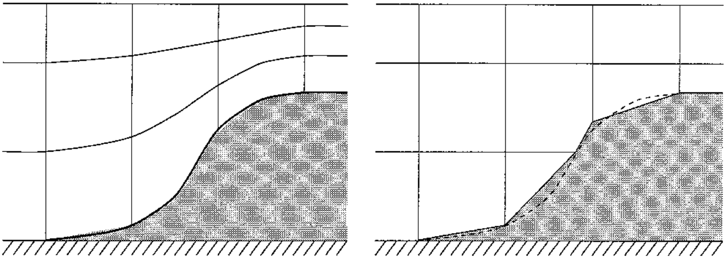

Figure: Representation of a smoothly varying bottom (dashed line) in (left) a terrain-following coordinate model, and (right) a height coordinate model with piecewise constant slopes (cut-cells, shaved-cells)

Figure is from Adcroft et al. (1997).

→ The main reason is that the lower boundary condition is very simple when using terrain-following coordinates!

Super-cycling (also referred to as sub-cycling) of tracers

- Continuity equation for air is coupled with momentum and thermodynamic equations:

Super-cycling (also referred to as sub-cycling) of tracers

- Continuity equation for air is coupled with momentum and thermodynamic equations:
    - thermodynamic variables and other prognostic variables feed back on the velocity field

Super-cycling (also referred to as sub-cycling) of tracers

- Continuity equation for air is coupled with momentum and thermodynamic equations:
  - thermodynamic variables and other prognostic variables feed back on the velocity field
  - which, in turn, feeds back on the solution to the continuity equation.

Super-cycling (also referred to as sub-cycling) of tracers

- Continuity equation for air is coupled with momentum and thermodynamic equations:
  - thermodynamic variables and other prognostic variables feed back on the velocity field
  - which, in turn, feeds back on the solution to the continuity equation.
  - Hence the continuity equation for air can not be solved in isolation and one must obey the maximum allowable time-step restrictions imposed by the fastest waves in the system.

Super-cycling (also referred to as sub-cycling) of tracers

- Continuity equation for air is coupled with momentum and thermodynamic equations:
  - thermodynamic variables and other prognostic variables feed back on the velocity field
  - which, in turn, feeds back on the solution to the continuity equation.
  - Hence the continuity equation for air can not be solved in isolation and one must obey the maximum allowable time-step restrictions imposed by the fastest waves in the system.
- The tracer transport equation can be solved in isolation given prescribed winds and air densities, and is therefore not susceptible to the time-step restrictions imposed by the fastest waves in the system.

Super-cycling (also referred to as sub-cycling) of tracers

- Continuity equation for air is coupled with momentum and thermodynamic equations:
  - thermodynamic variables and other prognostic variables feed back on the velocity field
  - which, in turn, feeds back on the solution to the continuity equation.
  - Hence the continuity equation for air can not be solved in isolation and one must obey the maximum allowable time-step restrictions imposed by the fastest waves in the system.
- The tracer transport equation can be solved in isolation given prescribed winds and air densities, and is therefore not susceptible to the time-step restrictions imposed by the fastest waves in the system.
- For efficiency: Use longer time-step for continuity equation for tracers than for air.

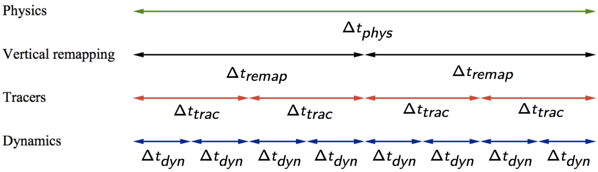

Δt_{dyn} = dynamics time-step; Δt_{trac} = tracer time-step; Δt_{remap} = remap time-step; Δt_{phys} = physics time-step (typically 1800s)

Leads to a major 'speed-up' of dynamics (however, we have to be careful with algorithmic design so we don't violate mass-conservation and free-stream/constant preservation (see Appendix)

Time-steps and namelist variables to control time-steps

The finite-volume fluid flow solver is coded in terms of nested loops:

```
do iv = 1, nv !  vertical re-mapping sub-cycle loop
  do n = 1, n2 !  tracer sub-cycle loop
    do it = 1, nsplit !  dynamics sub-cycle loop

    enddo
  enddo
enddo
```

where nv,n2, and nsplit are defined in terms of 'fv_' namelist variables

```
nv = fv_nspltvrm
n2 = (fv_nspltrac+nv-1)/fv_nspltvrm
nsplit = (fv_nsplit+n2*fv_nspltvrm-1) / (n2*fv_nspltvrm)
```

and the time-steps are given by

Δt_{remap} = Δt_{phys} / fv_nspltvrm = 900s (in CAM 1°)
Δt_{trac} = Δt_{phys} / fv_nspltvrm*n2 = 900s (in CAM 1°)
Δt_{dyn} = Δt_{phys} / fv_nspltvrm*n2*fv_nsplit= 225s (in CAM 1°)

- CAM-FV uses a Lagrangian ('floating') vertical coordinate ξ.
- ξ is retained *ksplit* dynamics time-steps Δt_{dyn}.
- Hereafter the prognostic variables are remapped to the Eulerian vertical grid η.
- For horizontal resolution of 1° CAM $ksplit = 4$ and $\Delta t_{dyn} = 225s$
  $\Rightarrow$ vertical remapping time-step is $900s$
- Δt_{dyn} is chosen based on stability
  (limited by gravity wave speed in CAM; advective winds in WACCM)
- Meridians are converging towards the poles: to stabilize the model (and reduce noise) FFT filters are applied along latitudes North/South of approximately 36°N/S.

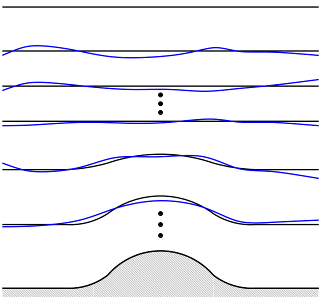

Vertical remapping

Vertical remapping algorithm matters!

Initial simulations with WACCM-SE-CSLAM showed almost no QBO signal compared to WACCM-FV

- It did not appear to be "tunable" with gravity wave tuning parameters

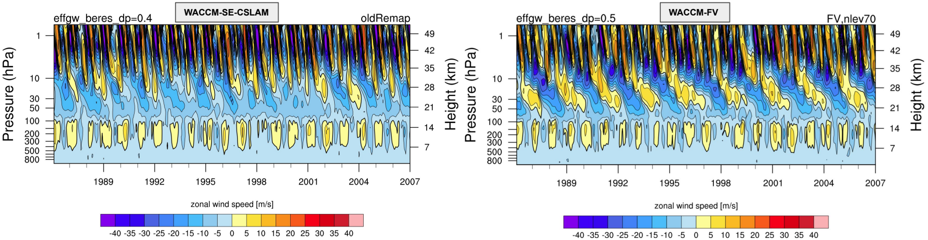

Vertical remapping

Vertical remapping algorithm matters!

Changing to FV3 vertical remapping for u,v,T,and water species improved QBO simulation significantly!

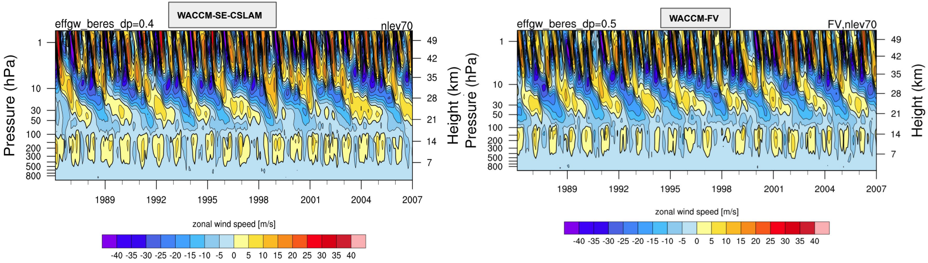

CAM-SE: (Lauritzen et al., 2018) Axial angular momentum conservation (Lauritzen et al., 2014)

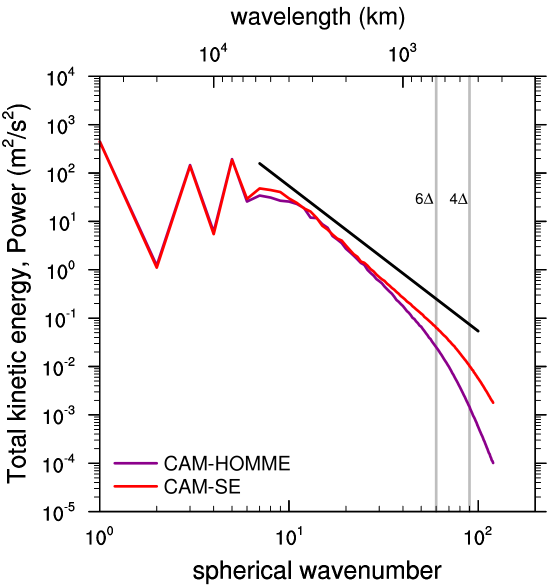

M=axial angular momentum integrated over the sphere. For a flat Earth $\frac{dM}{dt} = 0$

In the absence of mountain torque: $0 \sim \left(\frac{dM}{dt}\right)_{dyn} \ll \left(\frac{dM}{dt}\right)_{phys}$.

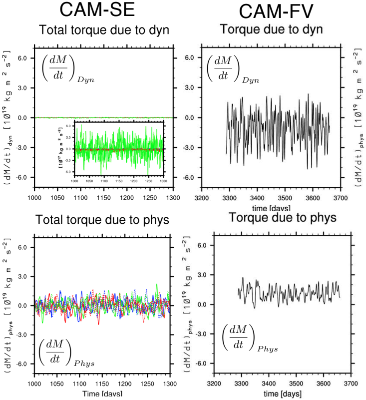

Is conservation of axial angular momentum important?

It is for super-rotating planets (Lebonnois et al., 2012). It is also argued to be important for Earth (Thuburn, 2008); possibly causing bias in CAM-FV (see T.Toniazzo's AMWG presentation from 2015: http://www.cesm.ucar.edu/events/wg-meetings/2017/presentations/amwg/toniazzo.pdf)

CAM-SE: (Lauritzen et al., 2018) Total energy conservation (Lauritzen and Williamson, 2019)

The total energy equation can be written on the form (Kasahara, 1974)

$$\frac{\partial}{\partial t}\left[\rho\left(\frac{\partial z}{\partial \eta^{(d)}}\right)(K+c_v T+gz)\right]+\nabla_{\eta^{(d)}}\cdot\left[\rho\vec{v}\left(\frac{\partial z}{\partial \eta^{(d)}}\right)(K+gz+c_p T)\right]=-\frac{\partial}{\partial \eta^{(d)}}\left(p\frac{\partial z}{\partial t}\right), \tag{9}$$

where c_p is heat capacity at constant pressure, z height, and $K=\frac{1}{2}\vec{v}\cdot\vec{v}$.

In z-based vertical coordinate (for a moment assume $\eta^{(d)}\equiv z$), then integrating energy equation in the vertical and using that z is constant at the model top (z_{top}) and surface (z_s) we get

$$\frac{\partial}{\partial t}\int_{z=z_s}^{z=z_{top}}(K+c_v T+gz)\,\rho dz+\nabla_z\cdot\int_{z=z_s}^{z=z_{top}}\vec{v}\,(K+gz+c_p T)\,\rho dz=0. \tag{10}$$

Note: clear separation of kinetic (K), potential (gz) and internal ($c_v T$) energy. Integrating in the horizontal over the entire sphere the flux term drops out, and it is clear that the total energy is conserved for the frictionless and adiabatic system of equations.

In a hybrid-sigma vertical coordinate and assuming that pressure model top is constant we get

$$\frac{1}{g}\frac{\partial}{\partial t}\int_{\eta=0}^{\eta=1}\left(\frac{\partial \mathcal{P}^{(d)}}{\partial \eta^{(d)}}\right)\sum_{\ell}\left[m^{(\ell)}\left(K+c_p^{(\ell)}T+\Phi_s\right)\right]d\eta^{(d)}=0 \tag{11}$$

where $\sum_\ell$ is sum over dry air, water vapor, cloud liquid, cloud ice, rain and snow ($\ell=$ ‘d‘, ‘wv‘, ‘cl‘, ‘ci‘, ‘rn‘, ‘sw‘’).

References I

Adcroft, A., Hill, C., and Marshall, J. (1997). Representation of topography by shaved cells in a height coordinate ocean model. *Mon. Wea. Rev.*, 125(9):2293–2315.

Arakawa, A. and Lamb, V. R. (1977). Computational design and the basic dynamical processes of the UCLA general circulation model. *Methods in Computational Physics*, 17:172–265.

Bannon, P. R. (2002). Theoretical foundations for models of moist convection. *J. Atmos. Sci.*, 59:1967–1982.

Bowen, P. and Thuburn, J. (2022a). Consistent and flexible thermodynamics in atmospheric models using internal energy as a thermodynamic potential. Part i: Equilibrium regime. under review.

Bowen, P. and Thuburn, J. (2022b). Consistent and flexible thermodynamics in atmospheric models using internal energy as a thermodynamic potential. Part ii: Non-equilibrium regime. under review at QJRMS.

Colella, P. and Woodward, P. R. (1984). The piecewise parabolic method (PPM) for gas-dynamical simulations. *J. Comput. Phys.*, 54:174–201.

Gross, M., Wan, H., Rasch, P. J., Caldwell, P. M., Williamson, D. L., Klocke, D., Jablonowski, C., Thatcher, D. R., Wood, N., Cullen, M., Beare, B., Willett, M., Lemarié, F., Blayo, E., Malardel, S., Termonia, P., Gassmann, A., Lauritzen, P. H., Johansen, H., Zarzycki, C. M., Sakaguchi, K., and Leung, R. (2018). Physics-dynamics coupling in weather, climate and earth system models: Challenges and recent progress. *Mon. Wea. Rev.*, 146:3505–3544.

Herrington, A. R., Lauritzen, P. H., Lofverstrom, M., Lipscomb, W. H., Gettelman, A., and Taylor, M. A. (2022). Impact of grids and dynamical cores in CESM2.2 on the surface mass balance of the Greenland ice sheet. *J. Adv. Model. Earth Syst.* revising.

Herrington, A. R., Lauritzen, P. H., Reed, K. A., Goldhaber, S., and Eaton, B. E. (2019). Exploring a lower-resolution physics grid in CAM-SE-CSLAM. *J. Adv. Model. Earth Syst.*, 0(0).

Herrington, A. R., Lauritzen, P. H., Taylor, M. A., Goldhaber, S., Eaton, B. E., Reed, K. A., and Ullrich, P. A. (2018). Physics-dynamics coupling with element-based high-order Galerkin methods: quasi equal-area physics grid. *Mon. Wea. Rev.*

Kasahara, A. (1974). Various vertical coordinate systems used for numerical weather prediction. *Mon. Wea. Rev.*, 102(7):509–522.

Lauritzen, P., Kevlahan, N.-R., Toniazzo, T., Eldred, C., Dubos, T., Gassmann, A., Larson, V., Jablonowski, C., Guba, O., Shipway, B., Harrop, B., Lemarié, F., Tailleux, R., Herrington, A., Large, W., Rasch, P., Donahue, A., Wan, H., Conley, A., and Bacmeister, J. (2022). Reconciling and improving formulations for thermodynamics and conservation principles in Earth System Models (ESMs). *J. Adv. Model. Earth Syst.* submitted.

Lauritzen, P. H. (2007). A stability analysis of finite-volume advection schemes permitting long time steps. *Mon. Wea. Rev.*, 135:2658–2673.

Lauritzen, P. H., Bacmeister, J. T., Dubos, T., Lebonnois, S., and Taylor, M. A. (2014). Held-Suarez simulations with the Community Atmosphere Model Spectral Element (CAM-SE) dynamical core: A global axial angular momentum analysis using Eulerian and floating Lagrangian vertical coordinates. *J. Adv. Model. Earth Syst.*, 6.

Lauritzen, P. H., Mirin, A., Truesdale, J., Raeder, K., Anderson, J., Bacmeister, J., and Neale, R. B. (2011a). Implementation of new diffusion/filtering operators in the CAM-FV dynamical core. *Int. J. High Perform. Comput. Appl.*

References II

Lauritzen, P. H., Nair, R., Herrington, A., Callaghan, P., Goldhaber, S., Dennis, J., Bacmeister, J. T., Eaton, B., Zarzycki, C., Taylor, M. A., Gettelman, A., Neale, R., Dobbins, B., Reed, K., and Dubos, T. (2018). NCAR release of CAM-SE in CESM2.0: A reformulation of the spectral-element dynamical core in dry-mass vertical coordinates with comprehensive treatment of condensates and energy. *J. Adv. Model. Earth Syst.*, 10(7):1537–1570.

Lauritzen, P. H., Taylor, M. A., Overfelt, J., Ullrich, P. A., Nair, R. D., Goldhaber, S., and Kelly, R. (2017). CAM-SE-CSLAM: Consistent coupling of a conservative semi-lagrangian finite-volume method with spectral element dynamics. *Mon. Wea. Rev.*, 145(3):833–855.

Lauritzen, P. H., Ullrich, P. A., and Nair, R. D. (2011b). Atmospheric transport schemes: desirable properties and a semi-Lagrangian view on finite-volume discretizations, in: P.H. Lauritzen, R.D. Nair, C. Jablonowski, M. Taylor (Eds.), Numerical techniques for global atmospheric models. *Lecture Notes in Computational Science and Engineering, Springer, 2011*, 80.

Lauritzen, P. H. and Williamson, D. L. (2019). A total energy error analysis of dynamical cores and physics-dynamics coupling in the Community Atmosphere Model (CAM). *J. Adv. Model. Earth Syst.*, 11(5):1309–1328.

Lebonnois, S., Covey, C., Grossman, A., Parish, H., Schubert, G., Walterscheid, R., Lauritzen, P. H., and Jablonowski, C. (2012). Angular momentum budget in general circulation models of superrotating atmospheres: A critical diagnostic. *J. Geo. Res.: Planets*, 117(E12):n/a–n/a.

Lin, S. J. (1997). Ti: A finite-volume integration method for computing pressure gradient force in general vertical coordinates. *Quart. J. Roy. Meteor. Soc.*, 123:1749–1762.

Lin, S.-J. (2004). A 'vertically Lagrangian' finite-volume dynamical core for global models. *Mon. Wea. Rev.*, 132:2293–2307.

Lin, S. J. and Rood, R. B. (1996). Multidimensional flux-form semi-Lagrangian transport schemes. *Mon. Wea. Rev.*, 124:2046–2070.

Lin, S.-J. and Rood, R. B. (1997). An explicit flux-form semi-Lagrangian shallow-water model on the sphere. *Q.J.R.Meteorol.Soc.*, 123:2477–2498.

Schär, C., Leuenberger, D., Fuhrer, O., Lüthi, D., and Girard, C. (2002). A new terrain-following vertical coordinate formulation for atmospheric prediction models. *Mon. Wea. Rev.*, 130(10):2459–2480.

Skamarock, W. (2011). Kinetic energy spectra and model filters, in: P.H. Lauritzen, R.D. Nair, C. Jablonowski, M. Taylor (Eds.), Numerical techniques for global atmospheric models. *Lecture Notes in Computational Science and Engineering, Springer*, 80.

Skamarock, W. C. (2008). A linear analysis of the NCAR CCSM finite-volume dynamical core. *Mon. Wea. Rev.*, 136:2112–2119.

Skamarock, W. C. and Klemp, J. B. (2008). A time-split nonhydrostatic atmospheric model for weather research and forecasting applications. *J. Comput. Phys.*, 227:3465–3485.

Skamarock, W. C., Klemp, J. B., Duda, M. G., Fowler, L. D., Park, S.-H., and Ringler, T. D. (2012). A multiscale nonhydrostatic atmospheric model using centroidal Voronoi tesselations and C-grid staggering. *Mon. Wea. Rev.*, 140:3090–3105.

Stevens, B., Satoh, and M., Auger, L. e. a. (2019). DYAMOND: the DYnamics of the Atmospheric general circulation Modeled On Non-hydrostatic Domains. *Prog Earth Planet Sci*, 6(61).

Taylor, M. A., Tribbia, J., and Iskandarani, M. (1997). The spectral element method for the shallow water equations on the sphere. *J. Comput. Phys.*, 130:92–108.

References III

Thomas, S. J. and Loft, R. D. (2005). The NCAR spectral element climate dynamical core: Semi-implicit Eulerian formulation. *J. Sci. Comput.*, 25:307–322.

Thuburn, J. (2008). Some conservation issues for the dynamical cores of NWP and climate models. *J. Comput. Phys.*, 227:3715–3730.

Thuburn, J. (2011). Some basic dynamics relevant to the design of atmospheric model dynamical cores, in: P.H. Lauritzen, R.D. Nair, C. Jablonowski, M. Taylor (Eds.), Numerical techniques for global atmospheric models. *Lecture Notes in Computational Science and Engineering, Springer*, 80.

van Leer, B. (1977). Towards the ultimate conservative difference scheme. IV: A new approach to numerical convection. *J. Comput. Phys.*, 23:276–299.

Whitehead, J., Jablonowski, C., Rood, R. B., and Lauritzen, P. H. (2011). A stability analysis of divergence damping on a latitude-longitude grid. *Mon. Wea. Rev.*, 139:2976–2993.

Williamson, D. L. (2002). Time-split versus process-split coupling of parameterizations and dynamical core. *Mon. Wea. Rev.*, 130:2024–2041.

Williamson, D. L. and Olson, J. G. (2003). Dependence of aqua-planet simulations on time step. *Quart. J. Roy. Meteor. Soc.*, 129(591):2049–2064.

Zarzycki, C. M., Jablonowski, C., and Taylor, M. A. (2014). Using variable-resolution meshes to model tropical cyclones in the community atmosphere model. *Mon. Wea. Rev.*, 142(3):1221–1239.